The Study on
Sulfur-Vanadium Pentoxide Composites as Cathode Materials for Magnesium Secondary Battery

by

Masashi INAMOTO

Graduate School of Saitama Institute of Technology

2016

PREFACE

Nowadays, secondary batteries that have high capacity and are intrinsically safe are required due to the significant progress of electronic devices, especially portable devices such as mobile phones, tablets and power sources for electric vehicles. The study on magnesium secondary batteries is still in the early stages. There are some impediments to the practical use of such devices: slower diffusion and intercalation of Mg^{2+} into cathode materials.

This is the thesis for a doctorate of Saitama Institute of Technology and relates to a vanadium pentoxide (V_2O_5) and sulfur composite as a magnesium secondary battery cathode, with the aim of developing a cathode material that would allow the repeated insertion/extraction of Mg^{2+} ions and would exhibit high capacity.

In Chapter 2 of the thesis, a V_2O_5 and sulfur composite synthesized by carbon felt-assisted microwave plasma of water (CF-MWP) that is symbolized as S-V_2O_5 showed a capacity of 300 mAh/g. It was found that the S-V_2O_5 particles were composed of two parts; an inner core of rigid V_2O_5 crystals covered by an approximately 10 nm thick surface layer similar to a V_2O_5 xerogel and incorporating sulfur. X-ray photoelectron spectroscopic analysis of the S-V_2O_5 electrode surface after charge and discharge indicated the presence of an electrolyte layer, representing a so-called solid electrolyte interphase (SEI), formed at the interface between the electrolyte and the S-V_2O_5 electrode surface. This SEI plays an important role in promoting the solid-state diffusion of Mg^{2+} ions. In Chapter 3, it was found the S-V_2O_5 achieved the higher capacity when combined with a metal oxide. The highest recorded capacity (420 mAh/g) was obtained upon the addition of manganese(II) oxide (MnO_2) to form the

composite SMn-V_2O_5. Structural assessments showed that the bulk of the SMn-V_2O_5 had an orthorhombic V_2O_5 structure, while the surface was composed of xerogel-like V_2O_5 and a solid solution of MnO_2 and sulfur. In Chapter 4, the author summarized work to prepare a V_2O_5 xerogel by microwave irradiation and the results of structural and electrochemical properties assessments. X-ray diffraction showed that the V_2O_5 xerogel prepared by microwave irradiation had a low degree of crystallinity, while charge-discharge tests revealed a specific capacity of 463 mAh/g. In Chapter 5, the preparation of a S-V_2O_5 gel using a new process and subsequent evaluation of the structure and electrode performance is discussed. Structural analysis showed that the bulk S-V_2O_5 gel adopted a V_2O_5 xerogel-like structure with a surface layer incorporating the sulfur and in a stable planar orientation, and that the surface had a reformed hard amorphous structure due to the CF-MWP treatment. Charge-discharge tests determined a specific capacity of 450 mAh/g, and cyclic voltammetry found almost perfect stability after the second cycle.

Through these Chapters, the S-V_2O_5 composite can be expected to function as a cathode material via Mg^{2+} ion insertion/extraction based on its enhanced cycling ability and structural stability. This study did not undertake a detailed analysis of the sulfur states in the S-V_2O_5, although such states are believed to have a significant effect on ion insertion/extraction. In future work, the effect of sulfur states on Mg^{2+} ion insertion/extraction should be assessed. I believe the results herein demonstrate the feasibility of using magnesium secondary batteries for practical applications based on further advances in the anode and electrolyte.

February 2016

Masashi Inamoto

ACKNOWLEDGEMENT

I wish to express my deepest gratitude to Professor Tatsuhiko Yajima of Saitama Institute of Technology for supervising and supporting this study. I would also like to thank Professor Uchiyama Shunichi, Professor Osamu Niwa, Professor Yasushi Hasebe and Associate Professor Hiroaki Matsuura for taking the time to review this thesis.

I also wish to sincerely thank Dr. Hideki Kurihara for his instruction in electrochemistry and microwave theory and for providing the opportunity to perform this study. Thanks are also extended to Mr. Teruyasu Mutaguchi of the Comprehensive Open Innovation Center of Saitama University (formerly the President of the Saitama Industrial Technology Center) and Mr. Yasuyuki Suzuki of the Saitama Industrial Technology Center for their assistance in entering the doctoral course and for providing guidance and encouragement. I am indebted to members of the Yajima Laboratory and to related people of the Saitama Industrial Technology Center for their support and advice during my research. Lastly, special thanks are due to my wife Sachiko Inamoto for giving me moral support.

February 2016

Masashi Inamoto

LIST OF PUBLICATIONS

1. M. Inamoto, H. Kurihara, T. Yajima, Electrode Performance of S-doped Vanadium Pentoxide as Cathode Active Material for Rechargeable Magnesium Battery, *Journal of the Surface Finishing Society of Japan*, **62** (10), 516-520 (2011), In Japanese.

2. M. Inamoto, H. Kurihara, T. Yajima, Electrode Performance of Vanadium Pentoxide Xerogel Prepared by Microwave Irradiation as Active Cathode Material for Rechargeable Magnesium batteries, *Electrochemistry*, **80** (6), 421-422 (2012).

3. M. Inamoto, H. Kurihara, T. Yajima, Vanadium pentoxide-based composite synthesized using microwave water plasma for cathode material in rechargeable magnesium batteries, *Materials*, **6** (10), 4514-4522 (2013).

4. M. Inamoto, H. Kurihara, T. Yajima, Electrode Performance of Sulfur-Doped Vanadium Pentoxide Gel Prepared by Microwave Irradiation for Rechargeable Magnesium Batteries, *Current Physical Chemistry*, **4** (3), 238-243 (2014).

CONTENTS

Chapter 1

General Introduction

1.1 Battery Introduction

There are two main types of batteries in everyday usage; primary and secondary (or rechargeable). Primary batteries are capable of one time use only and so are used until they are depleted and then disposed of. The most common primary batteries are alkaline manganese and zinc-air. In contrast, secondary batteries are constructed in a manner that allows for the original electrode materials to be restored by applying an external voltage. The first-generation secondary batteries, which are still in use, were lead-acid. More modern secondary batteries are the nickel-cadmium, nickel-metal hydride and lithium-ion types.

Circa 1980, secondary batteries appeared that incorporated so-called aqueous electrolytes, such as the nickel-cadmium and nickel-metal hydride batteries. Aqueous batteries such as these generate an electromotive force less than 1.5 V because of the electrolysis of water, and their applications are limited based on their size and weight. However, the demand for small rechargeable batteries has increased in association with the development and diffusion of portable electronic devices such as mobile phones.

The lithium-ion battery, the first nonaqueous electrolyte device, was subsequently developed by Yoshino *et al.*[1)] in the late 1980s, and the Sony Corporation put lithium-ion batteries into commercial use in the early 1990s.[2)] Lithium-ion batteries are now widely used in many practical applications.[3)] In fact, these are now the standard battery technology and have been optimized to a large extent. Recently, the use of lithium-ion batteries as power sources for hybrid and electric vehicles has grown rapidly as a means of reducing fossil fuel dependence.

As the smallest monovalent ion apart from H^+, lithium is an ideal ionic guest for

transferring electronic charges into various insertion hosts. However, there are only a limited number of countries that produce lithium (such as Chile, China and Argentina) and the element is often found in inaccessible locations, such as in concentrations of 0.04-1.16% in brine ponds, thus requiring almost a year for the final production of lithium carbonate. Notwithstanding this low accessibility, rechargeable lithium batteries will, for the time being, play a pivotal role as the most advanced electrochemical power sources.[4] In the meantime, many research institutions are developing non-lithium battery systems, such as sodium-ion, magnesium-ion and metal-air batteries, in order to ensure a sustainable supply of electrochemical energy storage devices.

1.2 Lithium Secondary Batteries

Even though the emphasis of this report is on magnesium batteries, the general workings of a lithium-ion battery will first be given, because this introduction serves as a good basis for the understanding of rechargeable ion transfer batteries. The main elements of a battery are the cathode, anode and electrolyte. In most modern batteries, a porous membrane is also present between the cathode and the anode to eliminate the possibility of electronic short-circuits, to minimize electrolyte usage and to increase the structural integrity of the device. The cathode and anode are the positive and negative electrodes, respectively, meaning that, upon discharge, electrons and cations flow from the anode to the cathode. Lithium secondary batteries have received significant attention because of their higher energy densities compared to Ni-Cd, Ni-metal hydride (MH) and Ni-H_2 batteries.

Cathode Materials

A lithium-ion battery employs so-called intercalation cathodes based on crystalline materials in which lithium is one of the major constituents. The key characteristics that are important for cathode materials are high ionic conductivity, favorable volume expansion upon discharge, high energy density and the ability to accommodate the extra charge and tension left in the structure when lithium ions are removed. The chemical equation summarizing the charge reaction at the cathode is as follows.

$$LiMO(s) \rightarrow Li^{+}(sol) + MO(s) + e- \qquad (1.1)$$

MO: metal oxide

Some typical cathode materials are presented in Table 1.1.

Table 1.1 typical lithium-ion cathode materials.[5)]

Material	Voltage vs. Li/Li^+	Theoretical Capacity	Usable Capacity
$LiCoO_2$	4.3 V	273.8 mAh/g	160 mAh/g
$LiNiO_2$	4.3 V	274.4 mAh/g	220 mAh/g
$LiFePO_4$	4.0 V	169.9 mAh/g	160 mAh/g
$LiMn_2O_4$	3.5 V	148.3 mAh/g	110 mAh/g

1.3 Magnesium Secondary Batteries

Figure 1-1 summarizes the operating principles of a magnesium secondary battery. Magnesium offers benefits as a battery constituent because it is divalent, i.e., the Mg^{2+} ion carries twice the charge of a Li ion.

Magnesium secondary batteries are a promising candidate to meet the future electrical energy storage needs of large-scale mobile and stationary devices, due to their advantages in terms of low cost as well as the high environmental abundance of magnesium metal and the divalent character of the Mg^{2+} ion. Among the possible alternatives to lithium-ion devices, magnesium secondary batteries have been much researched over the last two decades and magnesium is thought to represent the best metal anode material for high energy density batteries. The standard electrode potential of magnesium is -2.367 V. Although the theoretical gravimetric charge density of magnesium is lower than that of pure lithium (2233 mAh/g for Mg vs. 3884 mAh/g for Li), the divalent nature of magnesium ions presents a potential advantage in terms of volumetric capacity (3833 mAh/cm^3 for Mg vs. 2046 mAh/cm^3 for Li). Thus, while magnesium batteries might be heavier, they will be smaller. Despite its potential reactivity, magnesium is suitably stable in ambient air so as to allow handling and electrode preparation processes. Magnesium is also relatively benign and is the fifth most abundant element in the earth's crust; at present, 700,000 tons of magnesium are produced per year.

Despite these positive attributes, the development of magnesium ion technology has not kept pace with that of lithium ion technology. One critical issue impeding progress has been the development of a suitable electrolyte to enable the reversible release of

Mg^{2+} ions from a magnesium metal anode.[6] Unlike the Li^{+} ion conducting surface films formed by polar aprotic electrolyte solutions on Li metal electrodes, the surface films formed on magnesium metal often block the transport of Mg^{2+} ions. A second ongoing challenge is the development of cathode materials with high reversible capacity and adequate operating voltage under appropriate power output conditions. Due to the high valency of Mg^{2+} ions, the kinetics of solid state diffusion through inorganic cathode materials are slow, resulting in low reversible capacity and reduced power output.[7]

Significant progress has been made since Aurbach *et al.*[8] first reported a magnesium secondary battery prototype.[4),9] This has included new electrolytes[10] and recent advances in cathode materials.[11),12] These advancements have led to the study of magnesium secondary batteries all over the world.

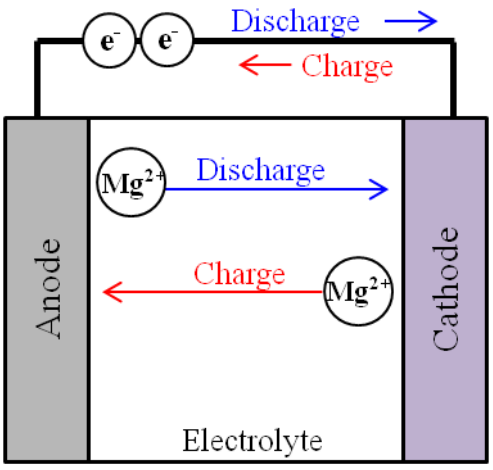

Figure 1-1 Schematic of magnesium secondary battery.

1.3.1 Cathode materials

With the recent increase in reports involving cathode materials for rechargeable magnesium batteries, it is important to assess the research in order to obtain new concepts for future study. Specifically, there have been many Mg^{2+} ion studies involving numerous cathode compositions and various phases. The choice of cathode materials for magnesium secondary batteries is extremely limited because divalent Mg^{2+} insertion/extraction in a host compound is difficult, presumably due to the stronger ionic interaction and differing charge redistribution of magnesium compared to the lithium ion.[13] Various cathode materials have been reported, however, including molybdenum sulfide (Mo_3S_4), vanadium pentoxide (V_2O_5), manganese oxide (MnO_2) and sulfur.

Mo_3S_4

Mo_3S_4 was first synthesized by Chevrel *et al.*[14] in 1974 and is therefore termed a Chevrel-type compound (Figure 1-2). It was investigated as a rechargeable magnesium battery electrode in 2000 by Aubach *et al.*,[8] who synthesized $CuMo_3S_4$ and removed the copper either chemically, with $FeCl_3$, or electrochemically. This compound was cycled against pure magnesium metal and it was found that, as a magnesium intercalation electrode, $MgMo_3S_4$ has a theoretical charge density of 121.8 mAh/g.

V_2O_5

V_2O_5 and the hydrated vanadium bronzes ($V_3O_8(H_2O)x$) were studied as possible magnesium intercalation hosts as early as 1995.[15] They exhibit high initial charge densities, upward of 200 mAh/g, but these decrease rapidly with cycling before stabilizing at approximately 80 mAh/g. Only V_2O_5 shows a large discharge capacity of

170 mAh/g, in an acetonitrile solution containing H_2O.[16] $Mg_XV_2O_5$ prepared by a sol gel method was shown to be quasi-reversible and had a delivered capacity above 250 mAh/g over several cycles.[17] Imamura *et al.* was able to fabricate a cathode in which Mg^{2+} was inserted in a manner similar to the usual Li^+ insertion.[18]

MnO_2

Zhang *et al.* reported potassium-stabilized manganese dioxide as a candidate cathode material.[19] The capacity of this cathode was 282 mAh/g on the initial discharge, although this value quickly faded to 134 mAh/g on the second cycle and continued to decrease with prolonged cycling. Spinel MnO_2 has also been synthesized using a microwave reactor[20] and the capacity of this material was found to be 80 mAh/g on the first discharge.

Sulfur

Kim *et al.* demonstrated the crystallization of electrochemically active species from the reaction between hexamethyldisilazide magnesium chloride and aluminum trichloride as a means of synthesizing a non-nucleophilic electrolyte. They confirmed that electrochemical conversion between sulfur and magnesium sulfide can be successfully performed using this electrolyte.[10]

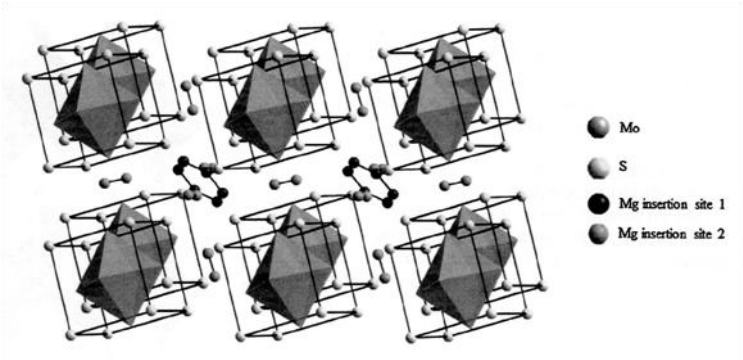

Figure 1-2 Chevrel phase of molybdenum sulfide.[21)]

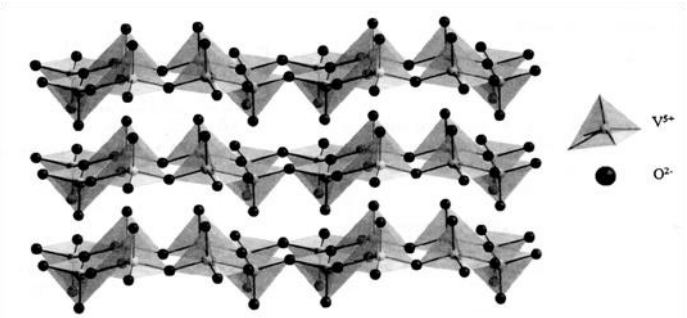

Figure 1-3 vanadium pentoxide.[7)]

1.4 Plasma Theory

1.4.1 Atmospheric Pressure Discharge Plasma

There are several methods of producing a plasma, but it is common to use atmospheric pressure discharge. Atmospheric pressure discharge occurs when a certain relationship holds true between two electrodes in a gas as a function of pressure and gap length, termed Paschen's Law. This relationship is given below.

$$Vs = f(Pd) \qquad (1.2)$$

P: gas pressure [Torr]

d: gap length [m]

An atmospheric pressure discharge plasma is an industrially effective technology because it requires no vacuum apparatus or exhaust system and is capable of high throughput.

The discharge in this process is a sudden and momentary electric current that flows between two objects at different electrical potentials. There are two types of discharge; glow discharge and arc discharge. A glow discharge apparatus consists of two electrodes in a cell held at low pressure, with an electrode potential of several hundred volts applied between the two electrodes. A small population of atoms within the cell is initially ionized and these ions are driven towards the cathode by the electric potential, while electrons are driven towards the anode by the same potential. The initial population of ions and electrons ionizes other atoms upon collision. As long as the

potential is maintained, a population of ions and electrons remains. The discharge current in this apparatus is less than 1 A. In contrast, arc discharge achieves a completely ionized state by thermal ionization. As the discharge current increases, the gas temperature is raised and thermal ionization occurs. A discharge current is typically more than 10 A.

Corona discharge is a continuous discharge that is caused by the unequal electric field around a needle electrode. There are different types of corona, including a glow corona, which regularly occurs in the region of the electrode, and a streamer corona, which develops linearly and occurs intermittently and can inflict damage on electrodes. Corona discharge is unsuitable for gaseous processing, since it is generated in a linear space. Finally, barrier discharge devices consist of two electrodes with a dielectric layer set between the two electrodes. Barrier discharge is generated by the application of an alternating voltage. In this device, the dielectric layer prevents damage to the electrodes by streamer coronas.

A plasma is a state in which electrons and cations coexist while maintaining micro electrical neutrality, and is often referred to as the fourth state of matter. A plasma is usually generated by applying energy to compounds in the vapor state, and combustion, discharge, nuclear radiation and laser beams are used as energy sources for plasma generation. Discharge is the most commonly used energy source. A glow discharge plasma is a non-equilibrium plasma; the electron temperature is several eV, the electron density ranges from 10^{9} to 10^{11} cm^{-3}, the ion temperature is several 0.1 eV and the gas temperature is several 0.01 eV. An arc plasma, however, is a thermal plasma; the electron temperature is several eV, the electron density ranges from 10^{15} to 10^{17} cm^{-3} and the ion and gas temperature are several eV, corresponding to 1000 °C. Therefore,

the apparatus for treatment using an arc plasma is difficult to manufacture.

Atmospheric pressure plasmas are used in a variety of materials processing techniques.[22)] Atmospheric pressure plasma devices can provide a crucial advantage over low pressure plasmas because they eliminate complications introduced by the need for vacuum. This technique therefore has a number of applications, such as high temperature materials processing and ozone production for water purification.

1.4.2 Atmosphere Pressure Discharge Plasma Using Carbon Felt

In the present work, atmospheric pressure microwave discharge (APMD) was generated by the microwave irradiation of two pieces of carbon felt (CF), upon which the temperature between the CF pieces increased. The temperature between the CF pieces was raised to more than 1000 °C after 10 sec of microwave irradiation[3)] and the associated discharge and heating can induce various reactions.

CF is a type of three-dimensional carbon fiber material. It has a large effective surface area (2500 °C calcined CF: 1.6 m^2/g), high mechanical strength and high conductivity (2500 °C calcined CF: 50 mΩ cm). In this study, therefore, CF was used as the electrode to obtain highly efficient electrolysis. Photographic, optical micrograph and SEM micrograph images of a CF specimen are shown in Figure 1-4. From these images, it can be seen that many cut ends of carbon fibers project from a cut surface, with air gaps between the fibers. CF is thus highly porous and so has significant insulating properties.

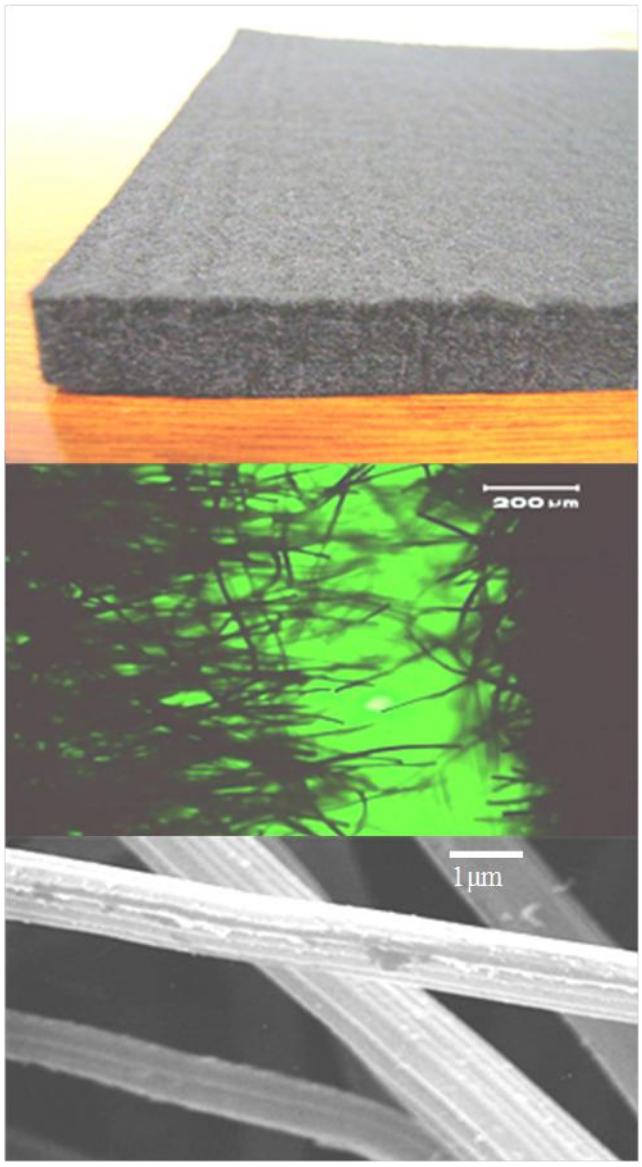

Figure 1-4 Photograph (a), optical microscope image (b) and SEM image (c) of CF.

1.4.3 Carbon-felt Microwave Water Plasma (CF-MWP)

As noted, this work employed an atmospheric pressure discharge plasma using carbon felt as a means of easily generating a plasma under reduced pressure. A schematic of the carbon-felt microwave water plasma (CF-MWP) device is provided in Figure 1-5a. This apparatus is constructed by first wetting a quantity of the raw material to be processed, after which it is placed between two pieces of CF. The resulting construction is placed in a glass vessel that can be placed under vacuum. The raw material in the vessel is subsequently irradiated with 2.45 GHz microwaves under reduced pressure and a water plasma is formed in response to the electric discharge between the two CF pieces (Figures 1-5b, 5c). The water plasma uniformly treats the raw material because water is homogeneously distributed throughout the material. Another characteristic of CF-MWP is that the temperature rise is very rapid and arrives at a thermal equilibrium state. Because of these characteristics, CF-MWP synthesis proceeds via inhibited oxidation and/or reduction of the raw material.

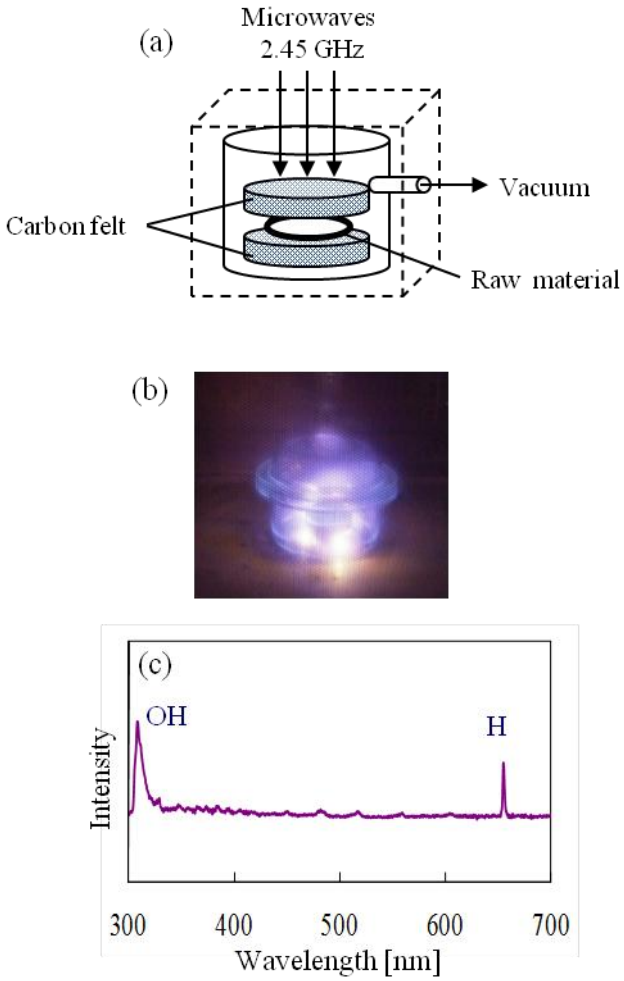

Figure 1-5 Schematic diagram (a), photograph (b), and Emission spectrum (c) of CF-MWP.

1.5 Background of this study

At present, secondary batteries that have high capacity and are intrinsically safe are required due to the significant progress of electronic devices, especially portable devices such as mobile phones and tablets, and as power source for electric vehicles. Magnesium secondary, lithium-sulfur and lithium-air batteries are all being developed as next-generation devices to satisfy these requirements. Of these, the magnesium secondary battery is the most promising based on the anticipated safety advantage.

At the moment, the study of magnesium secondary batteries is in the early stages. There are two main impediments to the practical use of such devices: (1) slower diffusion and intercalation of Mg^{2+} into cathode materials and (2) incompatibility between anodes and electrolytes due to the high polarizability of Mg^{2+}. Therefore, it is essential to design an adequate cathode and compatible anode and electrolyte.[24] Cathode materials for magnesium secondary battery candidates are limited to those employed in the lithium-ion batteries, and include Mo_3S_4, MnO_2 and V_2O_5 as described above. Levi *et al.* has suggested three main strategies to improve the kinetics of Mg transport in relevant cathode materials, using nanoscale materials, hydrates or similar intercalation compounds or cluster-containing compounds that readily attain local electroneutrality.[11] A combination of the first and second strategies in a material, such as a V_2O_5 gel and its derivatives, can generate relatively high voltage and capacity, but the associated kinetics are insufficient for practical battery use because of the incomplete charge screening upon cation insertion. Nevertheless, the development of cathode materials using V_2O_5 has been studied for some time, and has even been considered with regard to lithium secondary batteries.[25] For this reason, the present work also focuses on V_2O_5.

Crystalline V_2O_5 consists of layers of V_2O_5-based polyhedra and this structure provides pathways for ion insertion and extraction. The insertion of Mg^{2+} into V_2O_5 is a slow process, possibly due to the concurrent chemical modification of the V_2O_5 crystal surface. In recent studies, various groups have investigated hydrated V_2O_5 xerogels[26] and aerogels[27] in which water molecules are bound between the layers of V_2O_5. It is reported that a V_2O_5 xerogel exhibits a high capacity.[28] However, some of the water molecules in this gel remain bound to the magnesium and are extracted from the lattice during charging, ultimately leading to structural failure of the crystal upon cycling and a diminished capacity after the first cycle.

1.6 Purpose and significance of this research

Layered V_2O_5 represents a stable structure and Mg^{2+} ions inserted into V_2O_5 layers are not readily extracted because of the chemical interactions between the Mg^{2+} ions and the V_2O_5 oxygen. Sulfur is known to have a high theoretical capacity (1672 mAh/g) but also has an unstable crystalline structure that may dissolve in the electrolyte upon extraction of Mg^{2+} ions from the sulfur. V_2O_5 with added sulfur has been studied as a cathode material for lithium batteries because of the unique charge-discharge properties of this material.[29)] However, the addition of sulfur requires a highly precise and well controlled synthesis.[29)]

In the work reported herein, an attempt was made to apply sulfur-vanadium pentoxide prepared by CF-MWP as a cathode material for used in magnesium secondary batteries. The goal was to develop a unique cathode material allowing the insertion/extraction of magnesium ions and exhibiting high capacity.

This thesis is presented in two parts. The first part (Chapters 2 to 3) explains the crystal core structure of a proposed V_2O_5 cathode, while the second part (Chapters 4 and 5) focuses on the design of a V_2O_5 cathode with a xerogel core structure. Chapter 1 serves as a general introduction and Chapter 6 presents conclusions.

Chapter 1 describes the characteristic of plasma-based synthesis and the possibilities suggested by previous studies of magnesium secondary batteries and V_2O_5 cathodes.

Chapter 2 (Electrode Performance of Sulfur-Vanadium Pentoxide Composite Cathode Materials) discusses the treatment of V_2O_5 and sulfur using CF-MWP to inhibit the reduction of V_2O_5 and the oxidation of sulfur, generating S-V_2O_5. The structure of S-V_2O_5 and the electrochemical characteristics of a S-V_2O_5 electrode are described.

In Chapter 3 (Electrode Performance of Vanadium Pentoxide-based Composite

Cathode Materials), the synthesis of V_2O_5 with sulfur and metal oxides (MnO_2, Mo_2O_3, Fe_2O_3, ZrO_2, NiO) using CF-MWP is detailed.

Chapter 4 (Electrode Performance of Vanadium Pentoxide Xerogel Prepared by Microwave Irradiation as an Active Cathode Material) involves the desorption of structural water from a V_2O_5 xerogel using microwave irradiation. The electrode performance of a V_2O_5 xerogel formed by microwave irradiation is discussed based on structural and electrochemical analyses.

In Chapter 5 (Electrode Performance of Sulfur-Doped Vanadium Pentoxide Gel Composite Cathode Materials), investigations of the electrochemical performance and structure of a S-V_2O_5 gel prepared by CF-MWP after mixing of a V_2O_5 xerogel and sulfur are detailed.

Chapter 6 presents conclusions and a general overview of study results and future prospects.

1.7 Reference for Chapter 1

1) A. Yoshino, K. Sanechika and T. Nakajima, US4668595 A (1987)

2) Y. Nishi, H. Azuma and A. Omaru, US4959281 A (1990)

3) S. Okamoto, T. Ichitsubo, T. Kawaguchi, Y. Kumagai, F. Oba, S. Yagi, K. Shimokawa, N. Goto, T. Doi and E. Matsubara, *Advanced Science*, **2** (8), 1-9 (2015)

4) H. D. Yoo, I. Shterenberg, Y. Gofer, G. Gershinsky, N. Pour and D. Aurbach, *Energy & Environmental Science*, **6** (8), 2265-2279 (2013)

5) M. Yoshio, R.J. Brodd and A. Kozawa, editors. *Lithium-ion batteries Science and Technologies* (2009)

6) P. Novák, R. Imhof and O. Haas, *Electrochim. Acta*, **45** (1-2), 351-367 (1999)

7) M. M. Huie, D. C. Bock, E. S. Takeuchi, A. C. Marschilok and K. J. Takeuchi, *Coord. Chem. Rev.*, **287**, 15-27 (2015)

8) D. Aurbach, Z. Lu, A. Schechter, Y. Gofer, H. Gizbar, R. Turgeman, Y. Cohen, M. Moshkovich and E. Levi, *Nature*, **407** (6805), 724-727 (2000)

9) D. Aurbach, G. S. Suresh, E. Levi, A. Mitelman, O. Mizrahi, O. Chusid and M. Brunelli, *Adv. Mater.*, **19** (23), 4260-4267 (2007)

10) H. S. Kim, T. S. Arthur, G. D. Allred, J. Zajicek, J. G. Newman, A. E. Rodnyansky, A. G. Oliver, W. C. Boggess and J. Muldoon, *Nat Commun*, **2**, 427 (2011)

11) E. Levi, Y. Gofer and D. Aurbach, *Chem. Mater.*, **22** (3), 860-868 (2010)

12) E. Lancry, E. Levi, Y. Gofer, M. D. Levi and D. Aurbach, *J. Solid State Electrochem.*, **9** (5), 259-266 (2005)

13) J. Muldoon, C. B. Bucur, A. G. Oliver, T. Sugimoto, M. Matsui, H. S. Kim, G. D. Allred, J. Zajicek and Y. Kotani, *Energy & Environmental Science*, **5** (3), 5941-5950

(2012)

14) R. Chevrel, M. Sergent and J. Prigent, *Mater. Res. Bull.*, **9** (11), 1487-1498 (1974)

15) P. Novák, W. Scheifele, F. Joho and O. Haas, *J. Electrochem. Soc.*, **142** (8), 2544-2550 (1995)

16) P. Novák and J. Desilvestro, *J. Electrochem. Soc.*, **140** (1), 140-144 (1993)

17) S. H. Lee, R. A. DiLeo, A. C. Marschilok, K. J. Takeuchi and E. S. Takeuchi, *ECS Electrochemistry Letters*, **3** (8), A87-A90 (2014)

18) D. Imamura and M. Miyayama, *Solid State Ionics*, **161** (1-2), 173-180 (2003)

19) R. Zhang, X. Yu, K.-W. Nam, C. Ling, T. S. Arthur, W. Song, A. M. Knapp, S. N. Ehrlich, X.-Q. Yang and M. Matsui, *Electrochem. Commun.*, **23**, 110-113 (2012)

20) H. Kurihara, T. Yajima and S. Suzuki, *Chem. Lett.*, **37** (3), 376-377 (2008)

21) E. Levi, E. Lancry, A. Mitelman, D. Aurbach, O. Isnard and D. Djurado, *Chem. Mater.*, **18** (16), 3705-3714 (2006)

22) A. Schutze, J. Y. Jeong, S. E. Babayan, J. Park, G. S. Selwyn and R. F. Hicks, *Plasma Science, IEEE Transactions on*, **26** (6), 1685-1694 (1998)

23) H. Kurihara, *Saitama Institute of Technology*, Ph.D., (2008)

24) Y. Liu, L. Jiao, Q. Wu, J. Du, Y. Zhao, Y. Si, Y. Wang and H. Yuan, *Journal of Materials Chemistry A*, **1** (19), 5822-5826 (2013)

25) Y. Li, J. Yao, E. Uchaker, M. Zhang, J. Tian, X. Liu and G. Cao, *The Journal of Physical Chemistry C*, **117** (45), 23507-23514 (2013)

26) C.-Y. Lee, A. C. Marschilok, A. Subramanian, K. J. Takeuchi and E. S. Takeuchi, *PCCP*, **13** (40), 18047-18054 (2011)

27) D. B. Le, S. Passerini, F. Coustier, J. Guo, T. Soderstrom, B. B. Owens and W. H. Smyrl, *Chem. Mater.*, **10** (3), 682-684 (1998)

28) D. Imamura, M. Miyayama, M. Hibino and T. Kudo, *J. Electrochem. Soc.*, **150** (6), A753-A758 (2003)

29) V. Gorchkov, P. Novák and O. Volkov, US6916579 B2 (2005)

Chapter 2

Electrode Performance of Sulfur-Vanadium Pentoxide Composite Cathode Materials

2.1 Introduction

High-density secondary batteries are expected to be used as power sources for electrical vehicles. Divalent cation secondary batteries are promising because they can produce twice the current per atom of lithium batteries and have a higher energy density. The beryllium ion, which has the largest theoretical capacity of divalent cations, is not a good secondary battery cathode material because it forms covalent bonds. On the other hand, the magnesium ion, which has the second largest theoretical capacity of divalent cations, is expected to be applied for secondary battery cathode materials because of its higher tendency to undergo ionic bonding compared with covalent bonding. Therefore, magnesium secondary batteries, which have a long history of research, have begun to draw attention for next-generation power storage applications. Magnesium is inexpensive, safe to handle, environmentally friendly, and naturally abundant.[1)]

However, Mg^{2+} ions form strong electrostatic interactions with anions, undergo slow diffusion into cathode materials, and are easily trapped at the cathode. In addition, the crystal structure of cathode materials deteriorates or the electrolyte degrades during cycles of insertion/desorption of Mg^{2+} ions on/from the cathode at high voltage. For these reasons, magnesium secondary batteries do not have a high capacity or a long cycle life.[2-6)]

Therefore, the commercial viability of magnesium secondary batteries requires cathode materials that are stable for the insertion/desorption of Mg^{2+} ions. There have been a limited number of materials available as cathodes for magnesium secondary batteries: metal oxides[7-11)] and sulfides[12-13)] have mainly been reported as cathode materials. Metal oxides have stable crystalline structures but easily trap Mg^{2+} ions. On

the other hand, metal sulfides do not easily trap Mg^{2+} ions; however, they tend to have unstable crystalline structures that could possibly dissolve in the electrolyte.

Therefore, we have investigated ways to resolve such problems by changing the crystalline structure of the surface through the addition of sulfur to a metal oxide. The conduction properties of sulfur, which are low, could be improved by mixing it with metal oxide and carrying out a heat treatment. Metal oxide such as vanadium pentoxide (V_2O_5) with added sulfur has been previously examined as a cathode material for lithium secondary batteries because it has promising charge-discharge depth properties.[14] However, the addition of sulfur requires high-precision control of the synthesis conditions.[14] In this chapter, we discuss the application of V_2O_5 with added sulfur (S-V_2O_5), prepared by the carbon-felt microwave water plasma (CF-MWP) technique, as a cathode material.[15,16] The electrode performance and structural analysis of S-V_2O_5, and the electrochemical behavior of the S-V_2O_5 electrode surface are reported.

2.2 Experimental

2.2.1 Synthesis of sulfur-vanadium pentoxide composite (S-V_2O_5)

V_2O_5 and sulfur were mixed in a molar ratio of 3:1 in a ball mill (P-6, Fritsch Co., Ltd.) under an air atmosphere. The composite was wetted down and then treated with CF-MWP. Figure 2-1 shows the experimental setup for the CF-MWP process. Specifically, 2.0 g of each raw material was placed between pieces of carbon felt (30 mm diameter) and a 500 W, 2.45 GHz microwave was used to irradiate the material under reduced pressure (0.001 MPa) for 2 min to synthesize S-V_2O_5. The structure and the binding state of S-V_2O_5 were measured using X-ray diffraction (XRD; RINT 2000, Rigaku Corp.), X-ray photoelectron spectroscopy (XPS; ESCA Quantum 2000, Ulvac-Phi, Inc.), Fourier transform infrared spectroscopy with an attached diffuse reflection system (DRS-FTIR; IRPrestige-21, DRS-8000A, Shimadzu Corp.), Raman spectroscopy (XploRA, Horiba, Ltd.), and transmission electron microscopy (TEM; HF2000, Hitachi High-Technologies Corp.).

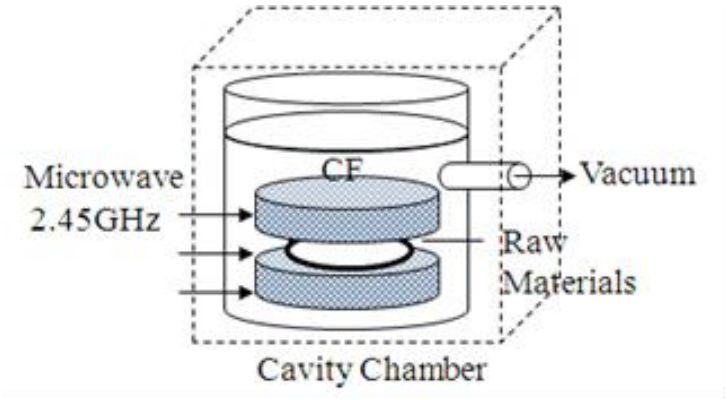

Figure 2-1 Experimental apparatus for S-V_2O_5 preparation using CF-MWP.

2.2.2 Electrochemical characteristics

The electrode performance was evaluated using three-electrode cells. The electrodes were prepared from a mixture of the cathode material, acetylene black, and a polyvinylidene fluoride binder with *N*-methyl-2-pyrrolidone with a weight ratio of 10:3:1. The resulting slurry was spread on carbon paper. The electrode was dried at 110 °C for 1.5 h. S-V_2O_5 was charged with magnesium ions and used as a counter electrode. A magnesium ribbon was used as the reference electrode. This electrode showed the same potential changes as a magnesium alloy plate. Namely, the S-V_2O_5 was had Mg^{2+} insertion at 30 mAh/g at 0.7 V *versus* Mg/Mg^{2+}. For the electrolyte solution, 0.3 M $Mg(ClO_4)_2$ and 1.8 M H_2O dissolved in propylene carbonate (PC) was used. Charge-discharge tests were conducted at a constant current of 60 mA/g (0.2 C). All trials were conducted at 20 °C.

2.2.3 Electrochemical behavior of the S-V_2O_5 electrode surface

Depth profiles of the electrode surface and chemical-bonding state after the first charge-discharge cycle were analyzed using X-ray photoelectron spectroscopy (XPS; ESCA Quantum 2000, Ulvac-Phi, Inc.). The discharged sample was prepared by discharging to 0.9 V, and the charged sample was prepared by discharging to 0.9 V and then charging to 2.4 V. For the electrolyte solution, 0.3 M $Mg(ClO_4)_2$ and 1.8 M H_2O dissolved in propylene carbonate was used. A magnesium ribbon was used as the reference electrode, and S-V_2O_5 was charged with magnesium ions and used as a counter electrode. XPS analysis was conducted using Ar^+ ions, an accelerating voltage of 4 kV, a pass energy of 23.50 eV, and a step size of 0.050 eV. All procedures from removal of the electrode from the cell to placement in the XPS spectrometer were conducted under a nitrogen atmosphere. All measurements were performed at room temperature (25 °C).

2.3 Results and discussion

2.3.1 Charge-discharge characteristics

The charge-discharge test results are shown in Figure 2-2 for V_2O_5, mixed V_2O_5 and sulfur, and S-V_2O_5. The capacity of the V_2O_5 electrode was 160 mAh g^{-1} at the first cycle but decreased to 70 mAh g^{-1} from the second cycle. This result corresponds with a previous report.[14] The discharge curve for the composite mixture of V_2O_5 and sulfur showed two plateaus at 1.4 V (P_1) and 1.0 V (P_2) *vs.* Mg/Mg^{2+}, which are attributed to V_2O_5 and sulfur, respectively. The P_2 plateau was observed only at the first discharge, and was not evident from the second discharge, which indicates that the sulfur is dissolved in the electrolyte when Mg^{2+} is extracted from the electrode during the first charge. The curve for S-V_2O_5 did not show a plateau but decreased linearly from 1.6 V to 1.0 V, in contrast to the composite mixture of V_2O_5 and sulfur. S-V_2O_5 has a high capacity (300 mAh g^{-1}) and good cycleability, which indicates that the surface of S-V_2O_5 is amorphous. The bulk of S-V_2O_5 has a V_2O_5 crystalline structure and the change in the S-V_2O_5 surface occurs not only due to the CF-MWP process, as discussed later. Therefore, these results indicate a reduction in the cycle degradation because the dissolution of sulfur is inhibited.

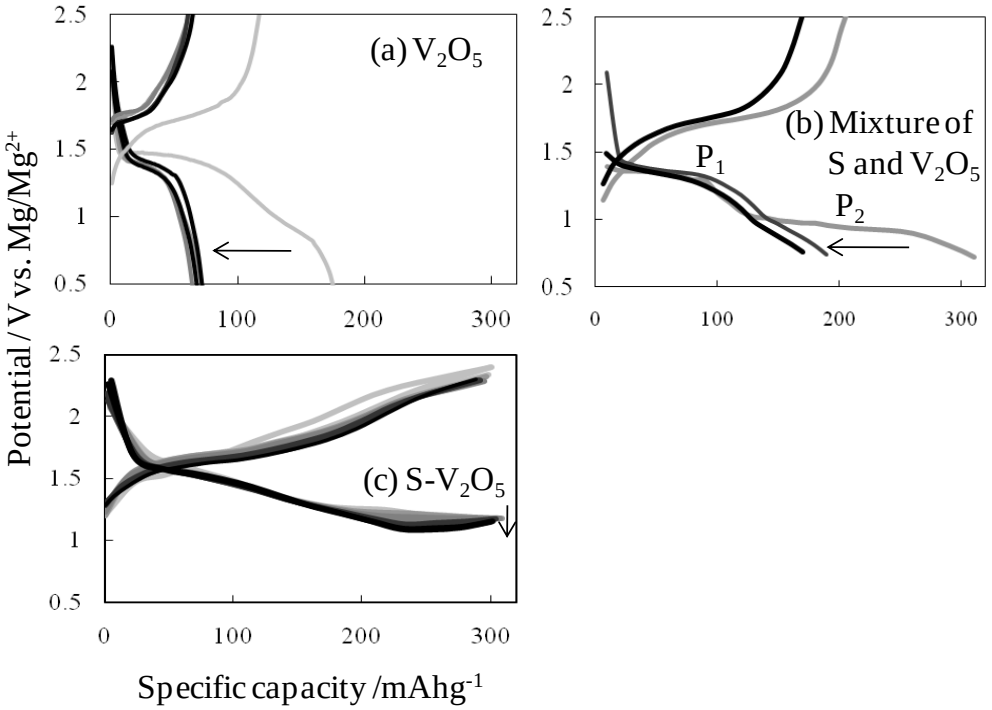

Figure 2-2 Charge-discharge curves: (a) V_2O_5, (b) Mixture of S and V_2O_5, and (c) S-V_2O_5.

2.3.2 Structural analysis

Figure 2-3 shows the emission spectrum of CF-MWP interacting with the raw materials. Intense H and OH spectral peaks mainly observed. These species may be derived from water molecules released from the raw materials and decomposed in CF-MWP. CF-MWP causes the surface color of the raw materials to change from orange to green. We attempted to steam the raw materials to synthesize S-V_2O_5 (100 °C, 2 min); however, the surface color did not change. The color change induced by CF-MWP indicates that the surface of raw materials produce S-V_2O_5.

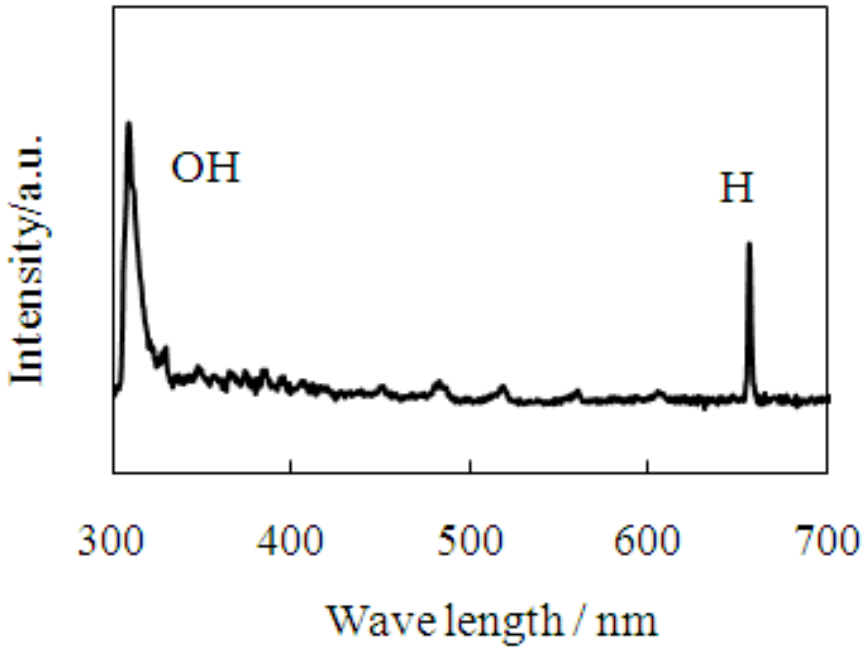

Figure 2-3 Emission spectrum of CF-MWP.

Figure 2-4 shows XRD patterns for the V_2O_5 standard and S-V_2O_5. The XRD pattern for S-V_2O_5 shows only peaks for V_2O_5 and sulfur without peak shifts or broadening, which indicates that CF-MWP does not change the V_2O_5 bulk structure. The composite mixture of V_2O_5 and sulfur is sintered and then generates VO_2 according to Equation (2.1). Figure 2-4 indicates that there is no reduction in bulk V_2O_5 using CF-MWP because the temperature of the reaction field during CF-MWP is probably low (under the boiling point of water in the standard-state).

$$S + 2V_2O_5 \rightarrow SO_2 + 2VO_2 \qquad (2.1)$$

Figure 2-5 shows Raman spectra for V_2O_5 and S-V_2O_5 measured at an excitation wavelength of 532 nm. The scattering intensity of S-V_2O_5 decreases compared with V_2O_5, which is probably due to a decrease in the scattering intensity from the particle surfaces. The fact may indicate that V_2O_5 particles in S-V_2O_5 system were covered with a low scattering intensity material. Figure 2-6 shows SEM images of V_2O_5 and S-V_2O_5. The V_2O_5 particles have angular geometry, whereas the S-V_2O_5 particles are spherically-agglomerated. These results indicate that CF-MWP changes the surface geometry of V_2O_5.

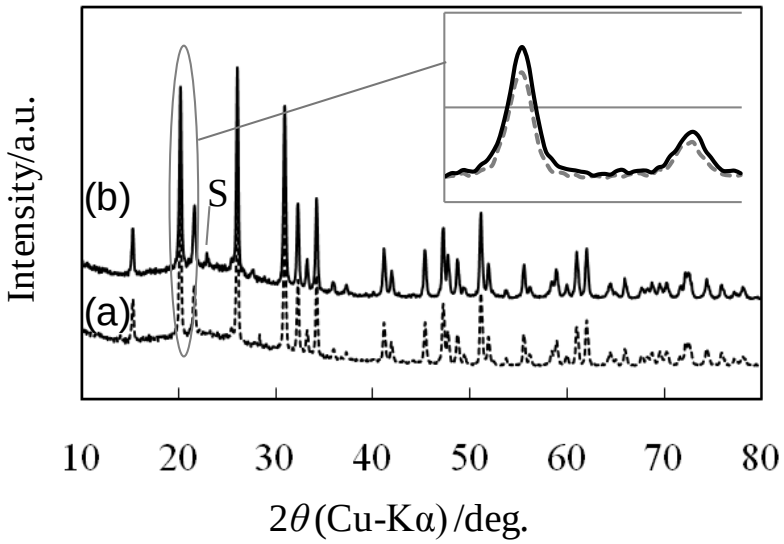

Figure 2-4 XRD patterns: (a) V_2O_5 (---), and (b) S-V_2O_5 (—).

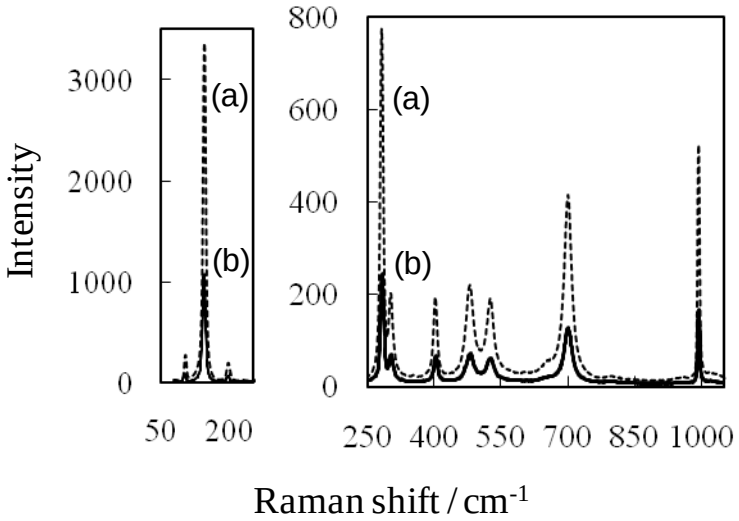

Figure 2-5 Raman spectra: (a) V_2O_5 (---), and (b) S-V_2O_5 (—).

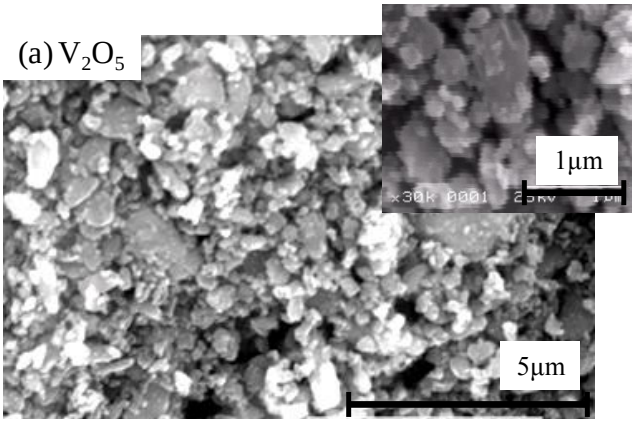

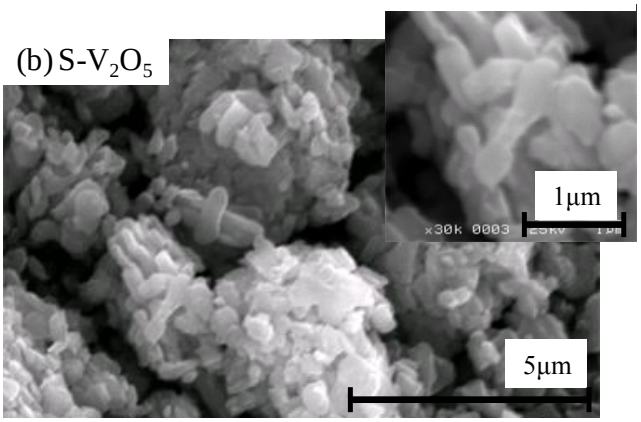

Figure 2-6 SEM images: (a) V_2O_5, and (b) S-V_2O_5.

Figure 2-7 shows S *2p* and V $2p_{3/2}$ XPS spectra for S-V_2O_5. The narrow S *2p* spectrum (Figure 2-7a) has a peak at 162.5 eV. The binding energy of this peak is lower than the of S_8, which indicates that the chemical-binding state of sulfur in S-V_2O_5 is different from that of S_8. The narrow V $2p_{3/2}$ spectrum (Figure 2-7b) has a peak at 160 eV. The binding energy of this peak is higher than that of V_2O_5. These results and the XRD analysis (Figure 2-4) suggest V-S chemical bonding near the surface of S-V_2O_5. The surface of S-V_2O_5 lowers the S-S binding energy due to the decreasing crystallinity of the sulfur.

Figure 2-8 shows DRS-FTIR spectra for V_2O_5 and S-V_2O_5. The spectrum for S-V_2O_5 has two peaks around 850 and 1020 cm^{-1}, which are attributed to V-O-V and V=O stretching vibrations, respectively. These peaks are broad toward the low wavenumber side, in contrast to the spectrum for V_2O_5. This indicates that the S-V_2O_5 surface has a broad range of V-O bond distances[17-20] due to its amorphous structure, which generated by sulfur doping with CF-MWP. The DRS attachment can detect information regarding the powder surface, and the results indicate the bulk of S-V_2O_5 has a crystalline V_2O_5 structure and the surface of S-V_2O_5 is amorphous.

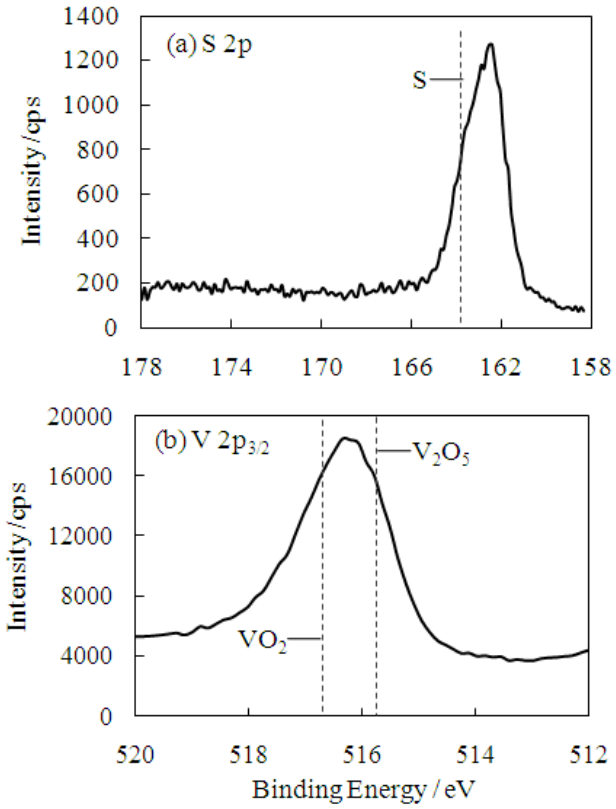

Figure 2-7 XPS narrow spectra of S-V_2O_5: (a) S 2p (narrow spectrum), and (b) V $2p_{3/2}$ (narrow spectrum).

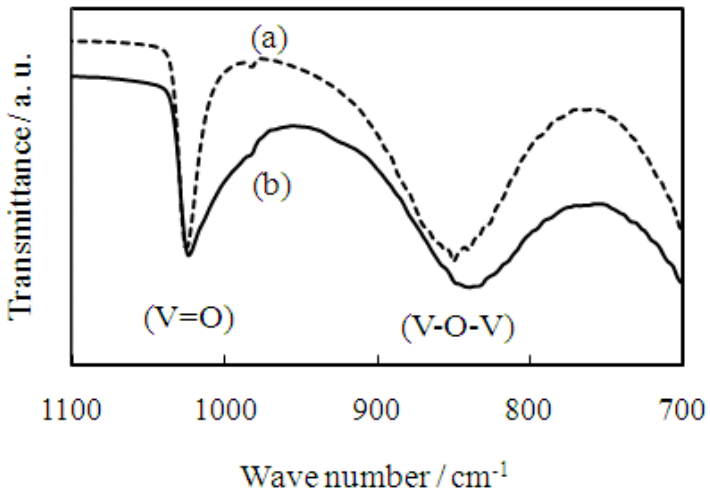

Figure 2-8 DRS-FTIR spectra: (a) V_2O_5 (---), and (b) S-V_2O_5 (—).

Figure 2-9 shows a TEM image and electron diffraction (ED) patterns of as-prepared S-V_2O_5 at two different points in the sample. The surface of the sample is composed of a thin 10-nm-thick layer (Figure 2-9a). The ED pattern of the S-V_2O_5 bulk indicates an orthorhombic V_2O_5 structure (Figure 2-9b), while that of the thin surface layer had a broader V-O band than that of orthorhombic V_2O_5 (Figure 2-9c).

V_2O_5 can easily absorb water from the atmosphere into the V_2O_5 layer, and this water interferes with the insertion/extraction of Mg^{2+} ions. However, the S-V_2O_5 surface accrues V-S bonds via the CF-MWP treatment, and the surface becomes amorphous with a xerogel structure. Therefore, the high capacity and a good cycle life of S-V_2O_5 are due to the special structure consisting of a bulk of crystalline V_2O_5 and an amorphous surface similar to V_2O_5 xerogel, which we call especially as the core-shell structure. The characteristic core-shell structure may inhibit the dissolution of sulfur into the electrolyte.

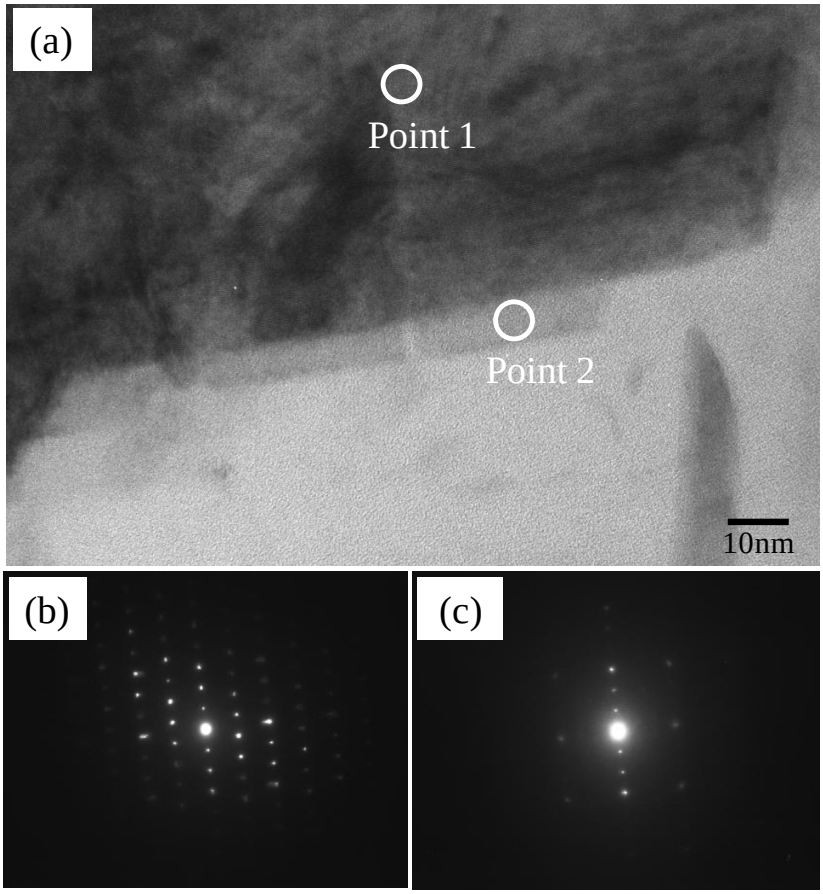

Figure 2-9 Characterization of S-V_2O_5; (a) is TEM image, (b) and (c) are ED patterns measured at point 1 and point 2 in (a), respectively.

2.3.3 Electrochemical characteristic of S-V_2O_5 electrode

Figure 2-10 shows Cole-Cole plots for V_2O_5 and S-V_2O_5 in the frequency range from 10 mHz to 20 kHz. The charge-transfer resistance (R_{ct}) of S-V_2O_5 is composed of two semicircles, in contrast to the one semicircle for V_2O_5. The R_{ct} of S-V_2O_5 is not a simple analogous circuit as with V_2O_5. This result indicates two transfer resistances of Mg^{2+} ions, which is consistent with the results shown in section 2.3.1 explaining the change in the surface structure of S-V_2O_5.

Figure 2-11 shows the discharge rate characteristics of S-V_2O_5. S-V_2O_5 maintained discharge potentials and specific discharge capacities, even though the discharge rate increases to C/2. Therefore, the magnesium secondary battery has high rate characteristics. Levi *et al.* proposed using hybrid intercalation compounds containing bound water or other additional anion groups that can presumably screen the charge of the inserted cations.[21] However, it is not possible to use the hybrid compound cathode at a high rate because the diffusion rate of Mg^{2+} ions decreases with repeated insertion in the system. On the other hand, it is reported that a Chevrel phase compound such as Mo_6S_8 shows high discharge rate characteristics because of immediately occurring the relocation of the charge between Mo and S and the ease of extracting inserted Mg^{2+} ions. For example, the discharge capacity of Mo_6S_8 is maintained at 100 mAh g^{-1} after 100 cycles at a rate of C/8.[22]

In this study, S-V_2O_5 is structurally classed as a hybrid compound cathode; however, it has high capacity at 300 mAh/g with a rate of C/2. S-V_2O_5 is not just a hybrid compound with a layered structure of V_2O_5 with inserted sulfur but forms an amorphous surface bonded with sulfur. This surface structure can easily transfer Mg^{2+} ions into

S-V_2O_5 because there is no passivated sulfur layer with low conductive properties but instead charge transfer between V_2O_5 and sulfur can take place.

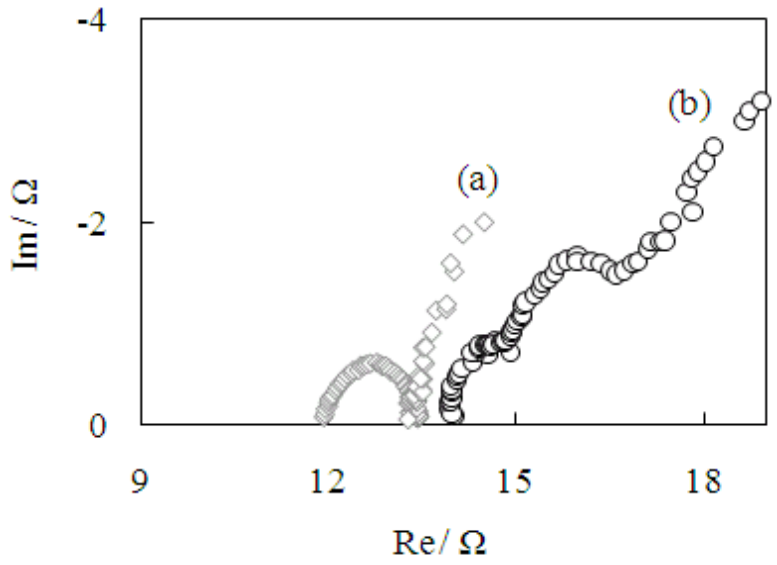

Figure 2-10 Cole-Cole plots: (a) V_2O_5 (◇), and (b) S-V_2O_5 (○).

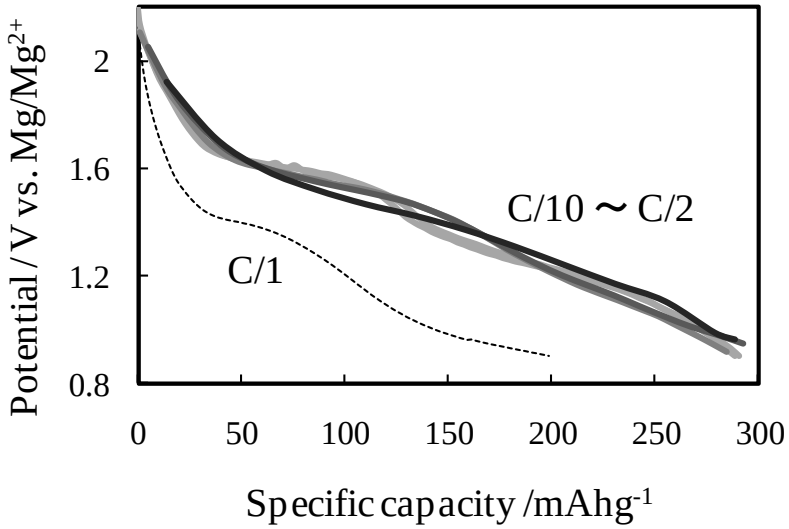

Figure 2-11 Rate profiles of S-V_2O_5.

2.3.4 Electrochemical behavior of the S-V_2O_5 electrode surface

Figure 2-12 shows XPS depth profiles for S-V_2O_5 in the upper five panels and those for V_2O_5 in the lower five panels. In the V *2p* depth profile for the S-V_2O_5 electrode after discharge (Figure 2-12e), the peak of vanadium is not shown, although the S-V_2O_5 electrode sample was sputtered ten times with Ar^+ ions. This result indicates that a solid electrolyte interphase (SEI) is probably formed at the interface between the electrolytic solution and the S-V_2O_5 electrode surface. In addition, the O *1s*, C *1s*, and Cl *2p* depth profiles indicate the formation of an SEI layer because each result shows a different structure before and after 10 times Ar^+ sputtering. The detected atoms of O, C and Cl may come from the electrolytic solution used in this study that was composed of the electrolyte $Mg(ClO_4)_2$ and the solvent PC whose chemical formula is $C_4H_6O_3$. The O *1s* depth profile of the S-V_2O_5 electrode after discharge (Figure 2-12c) has two peaks of 532 and 529 eV at the surface, which indicates the presence of CO_3^{2-} [23] and MgO[24], respectively. However, these peaks are not observed after charging (Figure 2-12d). The C *1s* depth profile of the S-V_2O_5 electrode after discharge (Figure 2-12g) indicates the formation of the SEI. The surface layer of the S-V_2O_5 electrode sample after discharge has a peak at 290 eV, although the sample after sputtering 10 times shows a peak at 285 eV. The peak at 290 eV indicates CO_3^{2-}, which indicates that the electrolyte layer includes $MgCO_3$ derived from the electrolyte.[25] The C *1s* peak at 290 eV is not observed after charge. The Cl *2p* depth profile of S-V_2O_5 after discharge (Figure 2-12i) shows partially overlapping peaks of Cl *2p*3/2 and *2p*1/2 at 198.4 eV, which indicates the presence of chloride ions (Cl^-).[26,27] The peaks for S-V_2O_5 after discharge and 10 times Ar^+ sputtering have strong intensity; however, the intensity of these peaks

decreased after charging (Figure 2-12j), which indicates that the SEI layer incorporates Cl^- ions during the discharge process. The Mg *2p* depth profile (Figure 2-12a) shows high intensity and broad peaks at 50.2 eV, and $MgCl_2$ (52.1 eV[28)]) is not observed in the electrolyte layer. These results demonstrate the formation of an SEI layer that is mainly composed of $MgCO_3$ and MgO and includes Cl^- at the interface between the electrolyte and the S-V_2O_5 surface after discharge. The S-V_2O_5 surface thus provides ease of Mg^{2+} insertion/extraction by the formation of the SEI layer.

The formation of Cl^- indicates the reduction of ClO_4^- in the electrolyte. The reduction reaction from ClO_4^- to ClO_3^- occurs easily at a low potential according to the following Equation 2.2. Cl^- ions can be included in the electrolyte layer when formed because a series of several chemical reactions occur at the S-V_2O_5 electrode surface during the discharge process (Equations 2.2-2.7).

$$ClO_4^- + H_2O + 2e^- \rightarrow ClO_3^- + 2OH^- \quad (E°= +0.17\ V) \quad (2.2)$$

$$ClO_3^- + H_2O + 2e^- \rightarrow ClO_2^- + 2OH^- \quad (E°= +0.35\ V) \quad (2.3)$$

$$ClO_2^- + H_2O + 2e^- \rightarrow ClO^- + 2OH^- \quad (E°= +0.59\ V) \quad (2.4)$$

$$ClO^- + H_2O + 2e^- \rightarrow Cl^- + 2OH^- \quad (E°= +0.90\ V) \quad (2.5)$$

$$ClO_3^- + 3H_2O + 6e^- \rightarrow Cl^- + 6OH^- \quad (E°= +0.62\ V) \quad (2.6)$$

$$ClO_2^- + 2H_2O + 4e^- \rightarrow Cl^- + 4OH^- \quad (E°= +0.76\ V) \quad (2.7)$$

The overall reduction reaction is:

$$ClO_4^- + 4H_2O + 8e^- \rightarrow Cl^- + 8OH^- \quad (2.8)$$

Considering that Mg^{2+} transportation involves H_2O molecules, the following scheme is proposed:

$$ClO_4^- + [Mg(H_2O)_4]^{2+} + 8e^- \rightarrow Mg^{2+} + Cl^- + 8OH^- \quad (2.9)$$

The S *2p* depth profiles shown in Figure 2-12(k, l) did not show the sulfur peak, and the molar ratio of V:S in S-V_2O_5 was 100:7.824. Therefore, it is difficult to observe the sulfur peak because the amount of sulfur involved in S-V_2O_5 was extremely small and below the detection limit. It should be noted that sulfur probably sublimes during the CF-MWP process. In addition, the raw material without added sulfur synthesized by CF-MWP did not show a change in the surface structure. These results indicate that the sulfur added to the raw material changes the surface structure of S-V_2O_5. Sulfur is known in high capacity cathode materials.[29] However, the higher capacity of S-V_2O_5 than V_2O_5 is not due to the addition of sulfur but due to the change in the S-V_2O_5 surface structure to that similar to a V_2O_5 xerogel.

On the other hand, the Mg *2p* XPS spectra of V_2O_5 after discharge (Figure 2-12m) showed small peaks at 50.5 eV near the surface and 50.8 eV in the bulk. After charging (Figure 2-12n), the peaks near the surface show a slight decrease in intensity. The O *1s* depth profile of V_2O_5 after discharge (Figure 2-12o) did not indicate $MgCO_3$ (532 eV) or MgO (529 eV), but the peak at 530.5 eV indicated the presence of V_2O_5 from the surface to the bulk. This is different from that for the S-V_2O_5 electrode analysis. These results indicate that the electrolyte layer formed at the S-V_2O_5 electrode surface is not formed at the V_2O_5 electrode surface.

Each V *2p* depth profile of S-V_2O_5 and V_2O_5 after discharge and charge (Figure 2-12e, f, q, r) shows a wide spectrum of V $2p_{1/2}$ (523-524 eV) and V $2p_{3/2}$ (516-517 eV). The wide spectrum indicates a mixture of different vanadium states: V^{5+} (V_2O_5, 517.6 eV), V^{4+} (V_2O_4, 516.3 eV), and V^{3+} (V_2O_3, 515.7 eV). The V $2p_{3/2}$ spectrum for vanadium metal shows a peak between 512.1 and 513.4 eV.[30] Therefore, it is difficult to recognize the oxidation-reduction of vanadium due to Mg^{2+} insertion/extraction.

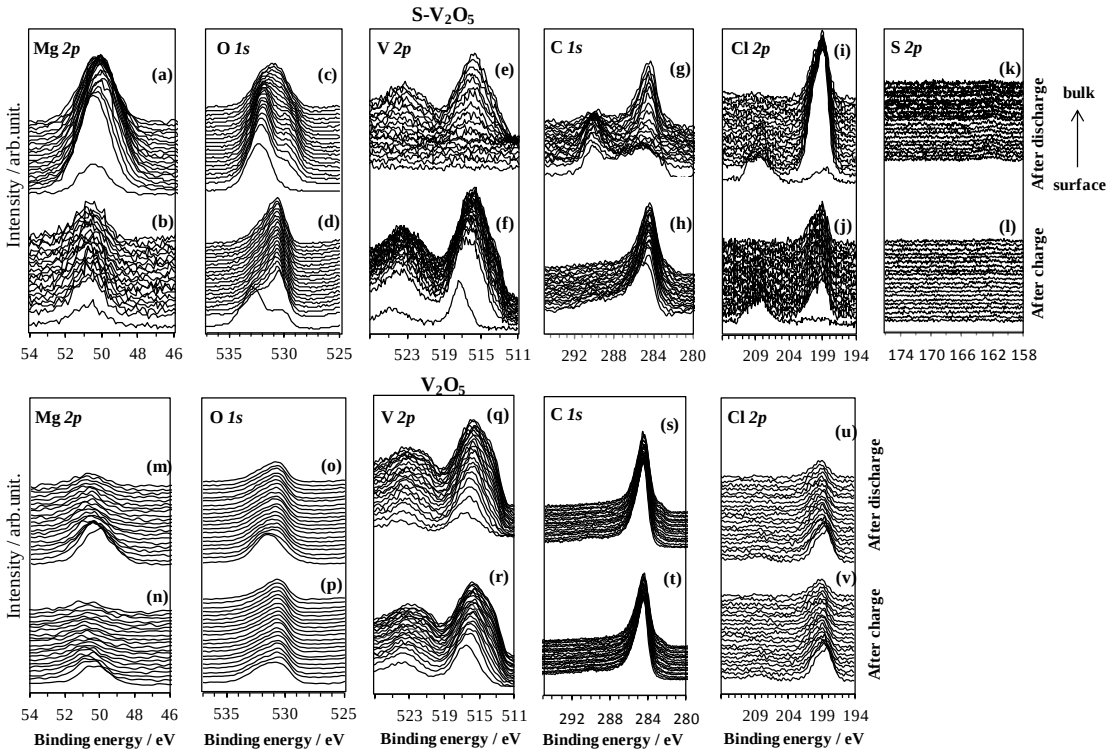

Figure 2-12 XPS profile in the Mg *2p* (a, b, m, n), O *1s* (c, d, o, p), V *2p* (e, f, q, r), C *1s* (g, h, s, t), Cl *2p* (I, j, u, v), and S *2p* (k, l) regions for S-V_2O_5 (a, b, c, d, e, f, g, h, i, j, k, l) and V_2O_5 (m, n, o, p, q, r, s, t, u, v) after discharge (a, c, e, g, i, k, m, o, q, s, u) and charge (b, d, f, h, j, l, n, p, r, t, v).

2.4 Conclusion

Conclusions on the synthesis of S-V_2O_5 using CF-MWP and its electrode characteristics are given in the following.

S-V_2O_5 has a characteristic structure which we call as the core-shell structure; a bulk structure of crystalline V_2O_5 and an amorphous surface structure similar to V_2O_5 xerogel. A magnesium secondary battery with the S-V_2O_5 cathode has high capacity (300 mAh/g) and increased cyclability. At a rate of C/2, the potential and specific discharge capacity were not significantly degraded. Electrochemical analysis of the discharge process indicated the presence of an SEI layer that is mainly composed of $MgCO_3$ and MgO, and includes Cl^- ions, which is formed at interface between the electrolyte and the S-V_2O_5 surface. The surface structure of S-V_2O_5 and the SEI layer facilitate the Mg^{2+} insertion/extraction process at the S-V_2O_5 surface. However, the sulfur added to the raw material did effect a significant change on the surface structure of S-V_2O_5 during the CF-MWP process.

2.5 Reference of Chapter 2

1) H. D. Yoo, I. Shterenberg, Y. Gofer, G. Gershinsky, N. Pour and D. Aurbach, *Energy & Environmental Science*, **6** (8), 2265-2279 (2013)

2) P. Novak, W. Scheifele and O. Haas, *J. Power Sources*, **54** (2), 479-482 (1995)

3) P. Novak and J. Desilvestro, *J.Electrochem, Soc*., **140** (1), 140-144 (1993)

4) D. Aurback, Z. Lu, A. Schemchter, Y. Goter, R. Tugeman, Y. Cohen, M. Moshkovlch and E. Levl, *Nature*, **407** (6805), 724-727 (2000)

5) P. Novak, V. Shklover and R. Nesper, *J. Phys. Chem.*, **185**, 51-68 (1994)

6) P. Novak, W. Scheifele, F. Joho and O. Haas, *J. Electrochem. Soc.*, **142** (8), 2544-2550 (1995)

7) L.Sanchez and J. P. Pereiraramos, *J. Mater. Chem*., **7** (3), 471-473 (1997)

8) Z. Feng, J. Yang, Y. NuLi and J. Wang, *J. Power Sources*, **184** (2), 604-607 (2008)

9) K. Makino, Y. Katayama, T. Miura and T. Kishi, *J. Power Sources*, **99** (1-2), 66-69 (2001)

10) N. Kumagai, S. Komaba, H. Sakai and N. Kumagai, *J. Power Sources*, **97-98**, 515-517 (2001)

11) L. Yu and X. Zhang, *Colloid Int. Sci.*, **278** (1), 160-165 (2004)

12) Z. L. Tao, L. N. Xu, X. L. Gou, J. Chen and H. T. Yuan, *Chem. Commun*., (18), 2080-2081 (2004)

13) A. Mitelman, M. D. Levi, E. Lancry, E. Levi and D. Aurbach, *Chem. Commun.*, (41), 4212-4214 (2007)

14) V. Gorchkov, P. Novak and O. Volkov, US Patent 6916579 (2005)

15) H. Kurihara and T. yajima, *Hyomen Gijutsu*, **57** (12), 895-895 (2006)

16) H. Kurihara and T. yajima, *Chem. Lett.*, **36** (4), 526-527 (2007)

17) M. Hibino, Y. Ikeda, Y. Noguchi, T. Kudo, *Seisan Kenkyu*, **52** (11), 516-522 (2000)

18) D. Imamura and M. Miyayama, *Solid State Ionics*, **161** (1-2), 173-180 (2003)

19) I. Stojkovića, N. Cvjetićanina, S. Markovićb, M. Mitrićc and S. Mentusa, *Acta Physica Pol. A*, **117** (5), 837-840 (2010)

20) N. Koshiba, K. Takada, M. Nakanishi and Z. Takehara, Denki Kagaku, **62** (10), 332-338 (1994).

21) E. Levi, Y. Gofer, D. Aurbach, *Chem. Mater.*, **22** (3), 860-868 (2010).

22) E. Lancry, E. Levi, Y. Gofer, M. Levi, D. Aurbach, *J. Solid State Electrochem*., **9** (5), 259-266 (2005).

23) S. Hwan Moon, T. Wook Heo, S. Young Park, J. Hyuk Kim and H. Joon Kim, *J. Electrochem. Soc.*, **154** (12), J408-J412 (2007)

24) O. Makita, S. Takagi and T. Gotoh, *Shinku*, **50** (3), 220-222 (2007)

25) K. Zhang, S. Wu, X. Wang, J. He, B. Sun, Y. Jia, T. Luo, F. Meng, Z. Jin, D. Lin, W. Shen, L. Kong and J. Liu, *J. Colloid Interface Sci.*, **446** (0), 194-202 (2015)

26) W. E. Morgan, J. R. Van Wazer and W. J. Stec, *J. Am. Chem. Soc.*, **95** (3), 751-755 (1973)

27) J. P. Contour, A. Salesse, M. Froment, M. Garreau, J. Thevenin and D. Warin, *J. Microsc. Spectrosc. Electron*, (4), 483-491 (1979)

28) S. Karakalos, A. Siokou and S. Ladas, *Appl. Surf. Sci.*, **255** (21), 8941-8946 (2009)

29) H. Wang, Y. Yang, Y. Liang, J. T. Robinson, Y. Li, A. Jackson, Y. Cui and H. Dai, *Nano Letters*, **11** (7), 2644-2647 (2011)

30) D. A. Shirley, R. L. Martin, S. P. Kowalczyk, F. R. MacFeely and L. Ley, *Phys. Rev. B*, (15), 544-552 (1977)

Chapter 3

Electrode Performance of Vanadium Pentoxide-based Composite Cathode Materials

3.1 Introduction

Recently, high-capacity secondary batteries have seen wide adoption as a power source for electric vehicles. Magnesium secondary batteries, which have been studied for a long time, have attracted attention for use in next-generation power storage applications. Aurbach *et al*. reported an electrolyte solution that allowed magnesium to dissolve and deposit reversibly.[1,2)]

However, there are a limited number of possible materials that can be used for the cathode of magnesium secondary batteries. In one case, Mg^{2+} is easily trapped in the cathode where it diffuses slowly, while in another, repetitive insertion/desorption of Mg^{2+} at the cathode by the use of high voltage can induce structural failure of the cathode or its dissolution into the electrolyte solution. Thus, one drawback of rechargeable magnesium batteries is the difficulty of maintaining their cycle characteristics due to diminishing capacity.[3,4)]

Therefore, there is high demand for cathode materials capable of stable insertion/desorption of Mg^{2+} to produce a feasible magnesium secondary battery. The most commonly studied cathode materials are metal oxides[5,6)] and metal sulfides.[7,8)] As a rule, metal oxides possess stable crystal architecture but easily trap Mg^{2+}. On the other hand, metal sulfides are less likely to trap Mg^{2+} because their structure is generally unstable. Sulfides generally have rather lower bond-energies than oxides. Therefore, they are considered to be unsuitable for use as the cathode material in lithium-ion batteries. Current research is advancing toward a solution to these problems.

3.3 Experimental

3.2.1 Preparation of Cathode Material by CF-MWP

Three kinds of composites were prepared. The first composites containing vanadium pentoxide (V_2O_5), sulfur, and a metal oxide (MnO_2, MoO_3, Fe_2O_3, NiO, or ZrO_2) at a molar ratio of 2:1:1 were prepared by mixing them in a ball mill (manufactured by Fritsch Co., Ltd., type P-6). The second composite containing V_2O_5, sulfur, and MnO_2 at a molar ratio of 2:1:1 was prepared as the same way to investigate the effect of an increased sulfur content. V_2O_5 and sulfur without metal oxide were also mixed in a ball mill to prepare the reference composite containing them at a molar ratio of 2:1, respectively (S-V_2O_5).

The composite materials were wetted down and left overnight, after which it was treated by low-temperature carbon-felt microwave water plasma (CF-MWP) generated using carbon felt and a 2.45 GHz microwave generator.[9,10)] Specifically, 2.0 g of each raw material were placed between pieces of carbon felt (30 mm in diameter) and a 500 W, 2.45 GHz microwave was used to irradiate the material under reduced pressure (0.001 MPa) for 2 min to synthesize the hybrid cathode materials. In this process, raw materials are treated by plasma formed from water in the raw materials as a result of electric discharge between the pieces of carbon felt. It is assumed that the distribution of water in the raw materials is sufficiently uniform that the composite is treated uniformly. Furthermore, although the process was performed under reduced pressure and at the evaporating temperature of water, the process did not induce reduction of V_2O_5 or the oxidation of sulfur.

3.2.2 Electrochemical Characteristics

Electrodes were prepared from a slurry mixture consisting of the cathode material, acetylene black, and a polyvinylidene fluoride binder in a weight ratio of 10:3:1 and mixed with N-methyl-2-pyrrolidone. The resulting slurry was spread on carbon paper and dried at 110 °C for 1.5 h to form an electrode. In the meanwhile, for preparing a counter electrode, S-V_2O_5 was charged with magnesium ions and used as that. This electrode showed the same potential changes as a magnesium alloy plate. A magnesium alloy plate was used as the reference electrode. For the electrolyte solution, 0.3 M $Mg(ClO_4)_2$ and 1.8 M H_2O dissolved in PC was used, and the electrode performance was evaluated using three-electrode cells. This electrolyte has been confirmed to allow smooth charge and discharge with metal oxides as cathode active materials.[4)] The stability of the Mg pseudo reference electrode was preliminarily confirmed to be stable by observation of the reproducibility of cyclic voltammograms with ferrocene using an electrolyte solution containing 0.2 M ferrocene, 0.3 M $Mg(ClO_4)_2$, and 1.8 M H_2O in PC solvent, and an electrochemical system with a magnesium alloy plate as the reference electrode, and platinum wires as working and counter electrodes. Charge-discharge tests were conducted between cut-off potentials from 2.4 V to 0.9 V *vs.* Mg/Mg^{2+} at a constant current of 60 mA/g (0.1 C). All trials were conducted at 25 °C.

3.2.3 Structural Analysis

The as-prepared samples were characterized using transmission electron microscopy (TEM; HF2000, Hitachi, Japan), energy-dispersive X-ray spectroscopy (EDX; Noran System SIX, Thermo Fisher Scientific, USA), micro-Raman spectroscopy (in Via Reflex/StreamLine, Renishaw, UK), X-ray photoelectron spectroscopy (XPS; ESCA Quantum 2000, Ulvac-Phi, Inc.), and inductively coupled plasma-mass spectrometry (ICP-MS; Agilent7500cs, Agilent Technologies). Raman spectroscopy measurements were conducted after the electrodes were prepared.

3.3 Results and Discussion

3.3.1 Electrochemical Characteristics

Figure 3-1 shows charge-discharge capacity curves for the batteries containing metal oxides (MnO_2, MoO_3, Fe_2O_3, NiO, and ZrO_2) as additives, which were 420, 320, 300, 290, and 230 mAh/g, respectively. The highest capacity was obtained for the electrode with MnO_2 (SMn-V_2O_5). The discharge curve for SMn-V_2O_5 decreased linearly from 1.5 V to 0.9 V *vs.* Mg/Mg^{2+}, which demonstrates that the surface of the SMn-V_2O_5 was amorphous with a structure similar to a xerogel; in this regard, it is similar to S-V_2O_5. Although the discharge curve obtained with added MoO_3 (Figure 3-1 (b)) decreased linearly from 1.5 V to 0.9 V *vs.* Mg/Mg^{2+}, the charge curve showed plateau potentials at around 1.8 V and 2.4 V. For the other electrode materials (Figure 3-1 (a), (c), (d) and (e)), a plateau potential appeared at 1.5 V, and each of the charge-discharge curves descended abruptly after the plateau potential. The cathode formed by the addition of NiO had the highest plateau potential at 1.65 V, different from the other electrode materials. This result shows that the addition of NiO may improve the high-voltage characteristics of the electrode material. Metal oxides other than MnO_2 inhibited the formation of an S-V_2O_5 amorphous structure and showed a plateau potential.

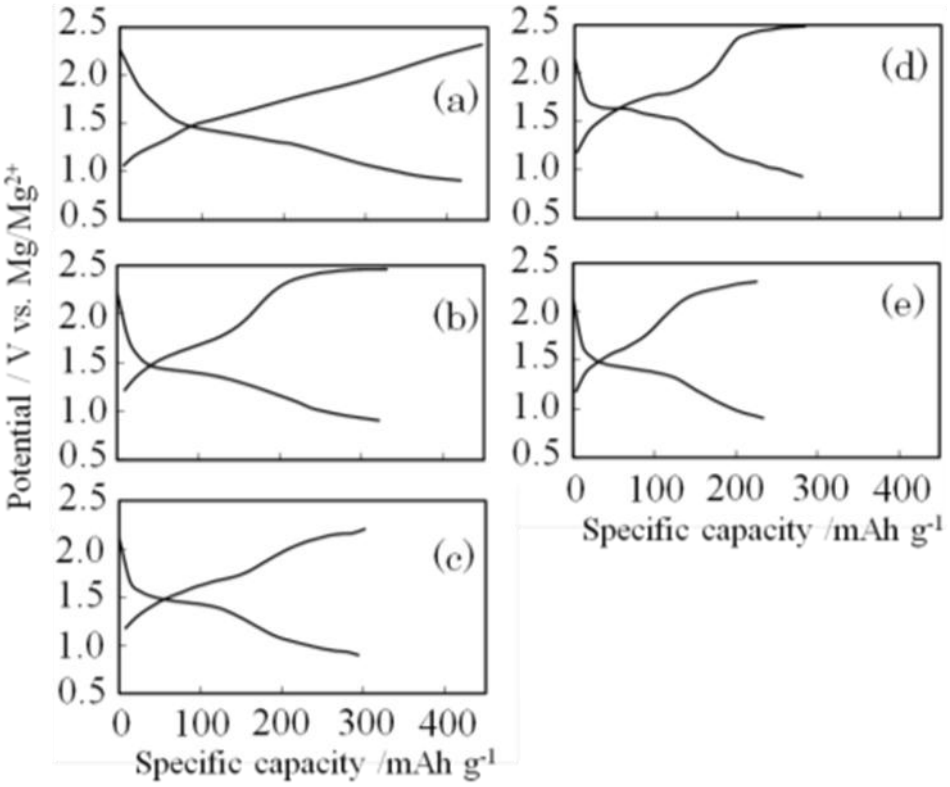

Figure 3-1 Charge-discharge curves at the second cycle for S-V_2O_5 with additives of (**a**) MnO_2, (**b**) MoO_3, (**c**) Fe_2O_3, (**d**) NiO, and (**e**) ZrO_2.

3.3.2 Structural Analysis

Figures 3-2 shows a TEM and electron beam diffraction patterns for SMn-V_2O_5, and Figure 3-3 shows the EDX spectra for SMn-V_2O_5 measured at two discrete points. The bulk of SMn-V_2O_5 produced clear electron diffraction and corresponds with the pattern for orthorhombic V_2O_5. Therefore, the bulk of the SMn-V_2O_5 maintained the V_2O_5 orthorhombic structure without degradation. The TEM image shows the surface of SMn-V_2O_5 as a thin layer with two types of morphology, shown as Points 1 and 2 in Figure 3-2. The diffraction image of Point 1 has a clear diffraction pattern and halo pattern, and is slightly broader than the pattern for orthorhombic V_2O_5. The halo pattern indicates an amorphous structure. The EDX spectrum measured at Point 1 shows a strong V peak, which indicates that Point 1 is a V_2O_5 xerogel or a similar structure. This is similar to the case for S-V_2O_5 (Figure 2-9). The diffraction image measured at Point 2 shows only a halo pattern, and the EDX spectrum shows peaks for manganese and sulfur. These results indicate that Point 2 has an amorphous structure that consists of only manganese and sulfur. Therefore, it is likely that Point 2 is a solid solution of MnO_2 and sulfur.

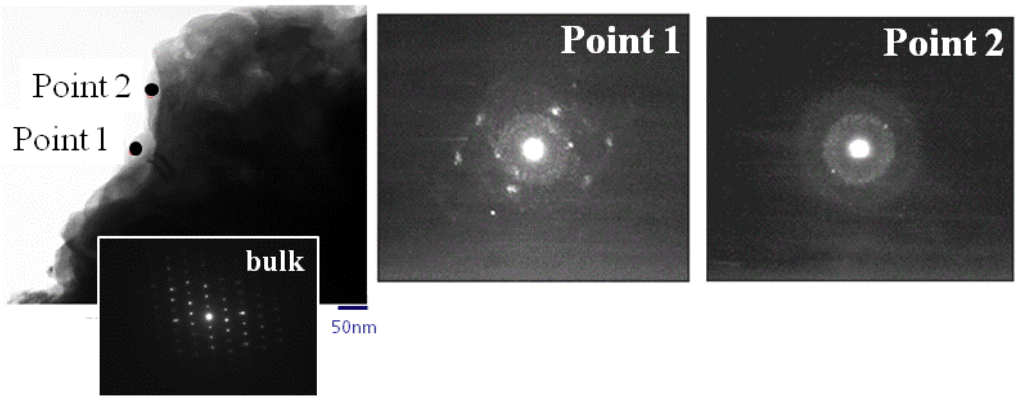

Figure 3-2 Transmission electron microscopy (TEM) of S-Mn-V_2O_5 and electron beam diffraction at Points 1 and 2.

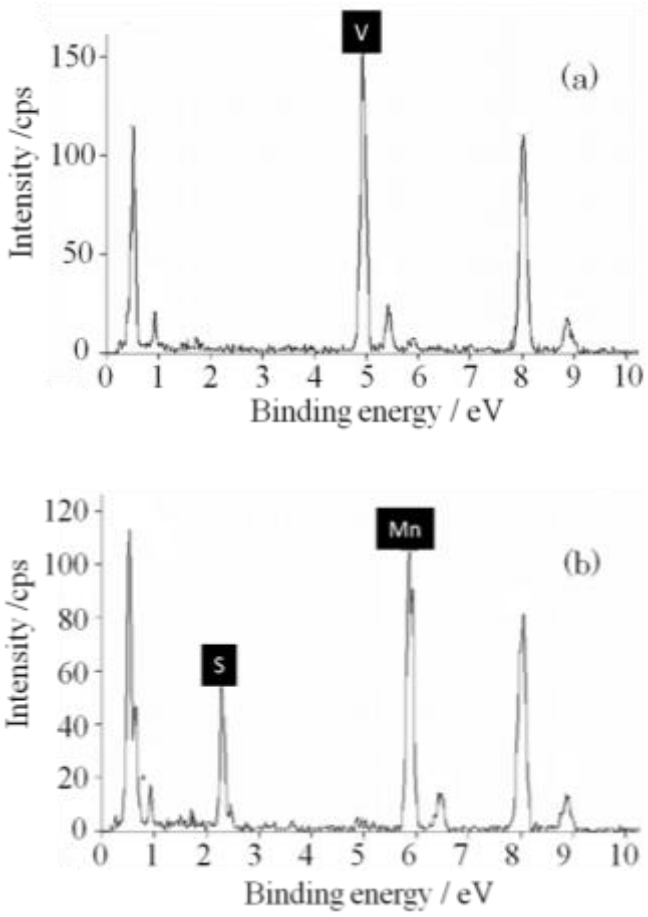

Figure 3-3 Energy dispersive X-ray spectrometry (EDX) at (**a**) Point 1; and (**b**) Point 2.

Figure 3-4 shows a micro-Raman spectrum and Raman images for the SMn-V_2O_5 electrode. Orthorhombic V_2O_5 peaks[11] and fluorescence are observed, whereas there are no MnO_2 and sulfur peaks. This result indicates fluorescence, possibly derived from MnO_2 and sulfur. Thus, during Raman spectroscopy, although the area of fluorescence was low in intensity for V_2O_5, the orthorhombic V_2O_5 and fluorescence area were separate. These results together with the results from TEM and EDX measurements indicate that the fluorescence area is a solid solution of MnO_2 and sulfur, which suggests that SMn-V_2O_5 consists of orthorhombic V_2O_5 in the bulk and the surface covered with the solid solution of MnO_2 and sulfur.

Figure 3-5 shows the XPS narrow spectrum of SMn-V_2O_5. The peaks for V $2p_{3/2}$ and S 2p are at the same positions as S-V_2O_5, which suggests a S-V bond-like state and indicates an amorphous structure as mentioned at the second chapter. The full width at half maximum (FWHM) of V $2p_{3/2}$ for SMn-V_2O_5 increased 2-fold compared to that for S-V_2O_5: 3.45 eV for SMn-V_2O_5 and 1.7 eV for S-V_2O_5. Therefore, it was considered that the oxidation state of V of SMn-V_2O_5 is slightly different than that in S-V_2O_5. The Mn $2p_{3/2}$ spectrum indicates the formation of a solid-solution with sulfur in accordance with TEM, EDX and Raman spectroscopy mentioned above. The ratio of manganese to sulfur was approximately 1:2 and remained constant when the amount of sulfur was increased five-fold. These results demonstrate that MnO_2 and sulfur are linked by mechanical force rather than by a chemical binding force. ICP-MS analysis indicated that the molar ratio of V:Mn:S was 100:6.8:14.4. The sulfur content in SMn-V_2O_5 was twice that in S-V_2O_5 (V:S = 100:7.8). The ratio of manganese to sulfur was approximately 1:2 in SMn-V_2O_5, which was determined by XPS analysis.

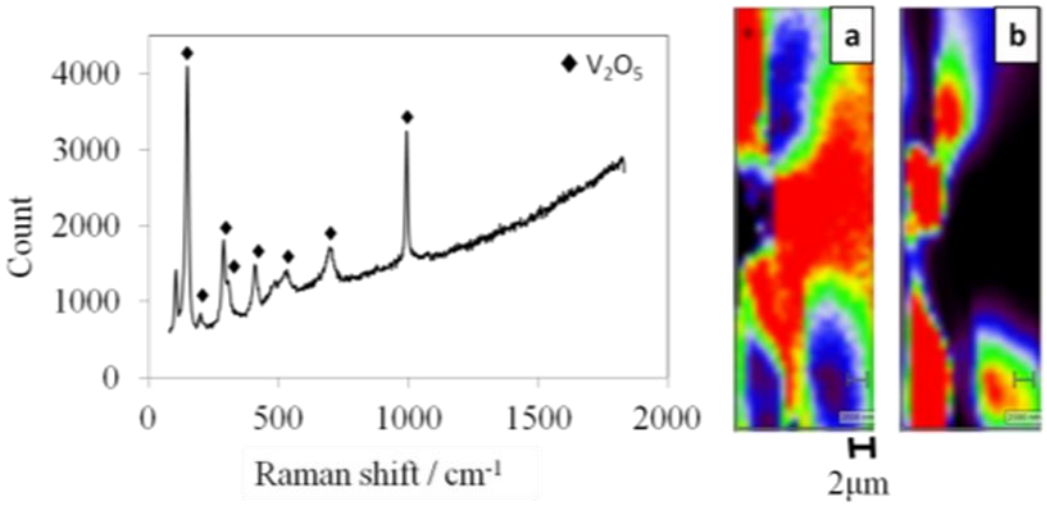

Figure 3-4 Raman spectroscopy of SMn-V_2O_5 and Raman images of the surface of the SMn-V_2O_5 of (**a**) V_2O_5; and (**b**) the fluorescence area.

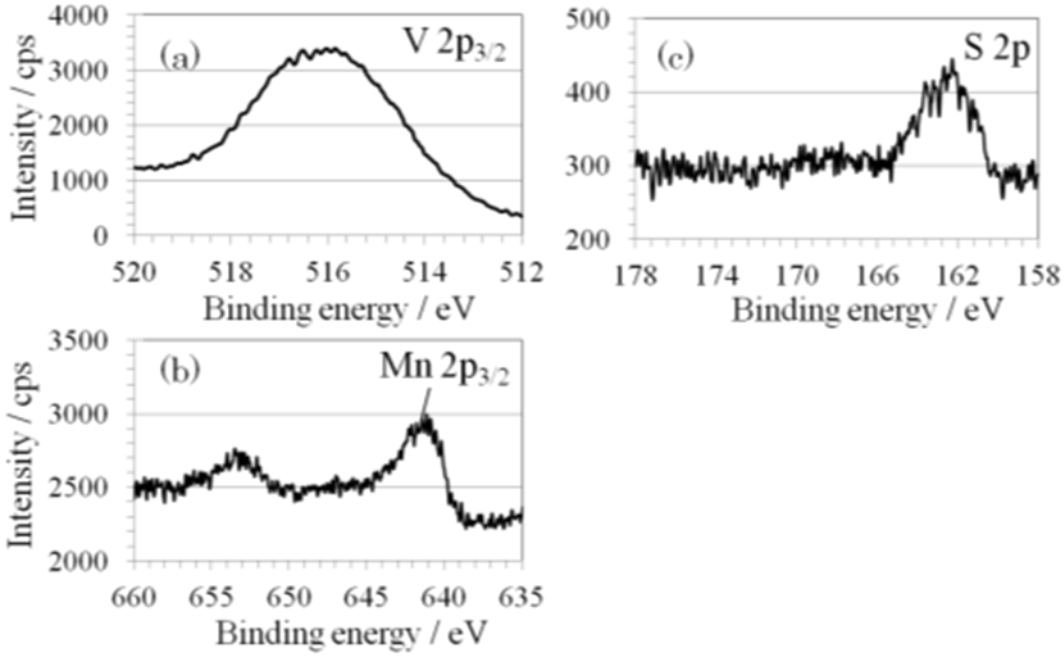

Figure 3-5 XPS narrow spectra of SMn-V_2O_5: (**a**) $V2p_{3/2}$; (**b**) $Mn2p_{3/2}$; and (**c**) S2p.

The following are balanced chemical reactions involving V_2O_5, MnO_2, and S, along with their theoretical capacities.

$$V_2O_5 + Mg^{2+} + 2e^- \rightarrow MgV_2O_5 \qquad 294\ mAh\ g^{-1} \qquad (1)$$

$$2MnO_2 + Mg^{2+} + 2e^- \rightarrow MgMn_2O_4 \qquad 307\ mAh\ g^{-1} \qquad (2)$$

$$S + Mg^{2+} + 2e^- \rightarrow MgS \qquad 1674\ mAh\ g^{-1} \qquad (3)$$

From the ICP-MS analysis and the three equations above, the average theoretical capacities of SMn-V_2O_5 and S-V_2O_5 through the surface to the bulk were calculated to be 458 and 393 mAh/g, respectively, i.e., the empirically obtained capacity of SMn-V_2O_5 is 91.7% of the theoretical capacity. The theoretical capacity of MnO_2 is as high as that of V_2O_5. Therefore, may be possible to achieve a high capacity for SMn-V_2O_5 by increasing the amount of sulfur.

3.4 Conclusions

As a cathode material for magnesium secondary batteries, S-V_2O_5 with an added metal oxide was synthesized using CF-MWP and its crystal structure and electrode characteristics were examined. The composite of V_2O_5, sulfur, and MnO_2 (SMn-V_2O_5) synthesized by CF-MWP demonstrated the highest capacity (420 mAh/g) of any of the prepared samples. Charge-discharge curves showed that the SMn-V_2O_5 capacity decreased linearly from 1.5 V to 0.9 V, whereas a plateau potential appeared at 1.5 V for the other electrodes. This result was interpreted to indicate that only SMn-V_2O_5 had a surface structure resembling a xerogel. The bulk of the SMn-V_2O_5 composite was orthorhombic V_2O_5, while the surface showed a xerogel-like structure of V_2O_5 and a solid solution of sulfur and MnO_2.

3.5 References of Chapter 3

1) D. Aurbach, Z. Lu, A. Schechter, Y. Gofer, H. Gizbar, R. Turgeman, Y. Cohen, M. Moshkovich and E. Levi, *Nature*, **407** (6805), 724–727 (2000)
2) D. Aurbach, Y. Cohen and M. Moshkovich, *Electrochem. Solid State Lett.*, **4** (8), A113–A116 (2001)
3) P. Novák, W. Scheifele and O. Haas, *J. Power Sources*, **54** (2), 479–482 (1995)
4) P. Novák, W. Scheifele, F. Joho and O. Haas, *J. Electrochem. Soc.*, **142** (8), 2544–2550 (1995)
5) P. Novák and J. Desilvestro, *J. Electrochem. Soc.*, **140** (1), 140–144 (1993)
6) Z. Feng, J. Yang, Y. NuLi and J. Wang, *J. Power Sources*, **184** (2), 604–609 (2008)
7) Z.L. Tao, L.N. Xu, X.L. Gou, J. Chen and H.T. Yuan, *Chem. Commun.*, (18), 2080–2081 (2004)
8) A. Mitelman, M.D. Levi, E. Lancry, E. Levi and D. Aurbach, *Chem. Commun.*, (41), 4212–4214 (2007)
9) M. Inamoto, H. Kurihara and T. Yajima, *Hyomen Gijutsu*, **62** (10), 516–520 (2011)
10) H. Kurihara and T. Yajima, *Chem. Lett.*, **36** (4), 526–527 (2007)
11) R. Baddour-Hadjean, M.B. Smirnov, K.S. Smirnov, V.Y. Kazimirov, J.M. Gallardo-Amores, U. Amador, M.E. Arroyo-de Dompablo and J.P. Pereira-Ramos, *Inorg. Chem.*, **51** (5), 3194–3201 (2012)

Chapter 4

Electrode Performance of Vanadium Pentoxide Xerogel Prepared by Microwave Irradiation as an Active Cathode Material

4.1 Introduction

Magnesium secondary batteries have been studied for a significant length of time, and are currently being considered for next generation power storage applications. This is partly because magnesium is low cost, safe to handle, environmentally friendly and naturally abundant.

However, there are only a limited number of materials available for use as the cathode in magnesium secondary batteries. Aurbach et al. reported an electrolyte solution that allows magnesium to dissolve and deposit reversibly,[1,2] while Novak et al. studied V_2O_5 as a potential cathode material.[3,4] Imamura et al. examined Mg^{2+} intercalation into a composite prepared from a V_2O_5 xerogel and carbon and determined that the V_2O_5/carbon composite had a large interlayer distance and short diffusion length compared to a V_2O_5 xerogel without carbon.[5] The present study focused on the drying of this V_2O_5 xerogel, which is known to develop narrow interlayer distances upon thermally-assisted drying above 50 °C.[5] Specifically, microwave (MW) irradiation under vacuum was employed to dry the V_2O_5 xerogel in an attempt to achieve greater interlayer distances than those that can be obtained by conventional heat treatments.

4.2 Experimental

The V_2O_5 xerogel was prepared by a sol-gel process. V_2O_5 (1 g) was added to a 10 wt% aqueous H_2O_2 solution (100 mL) with electromagnetic stirring and the resulting hydrogel was dried overnight at 70 °C in a dry oven until it became a dark brown xerogel. Thus, the V_2O_5 xerogel dried just at the surface, however still wetted in the bulk. This material was transferred to a glass vessel and subjected to MW irradiation (500 W, 2.45 GHz) for 4 min under vacuum. For comparison purposes, V_2O_5 xerogels were also dried at either 200 or 300 °C for 8 h. The structures of the dried xerogels were examined by X-ray diffraction (XRD; Rigaku, RINT 2000).

Electrodes were prepared using a 7:2:1 (by mass) mixture of V_2O_5 xerogel with acetylene black and polyvinylidene fluoride (PVdF) binder in the solvent N-methyl-2-pyrrolidone, followed by spreading the resulting slurry (5 mg per cm^2) on carbon paper. The resulting electrodes were dried at 110 °C for 1.5 h. Cyclic voltammetry (CV) data were obtained with three electrode cells using an electrochemical measurement system (Hokuto Denko, HZ-3000) with Ag/AgCl as the reference electrode and S-V_2O_5 prepared by our own method[6)] and charged with Mg^{2+} ions as a counter electrode. This electrode was found to exhibit the same potential changes as a magnesium alloy plate and thus a magnesium alloy plate was used as the reference electrode. Electrode performance in the three electrode cell was assessed using 0.3 M $Mg(ClO_4)_2$ dissolved in propylene carbonate (PC) as the electrolytic solution. Charge-discharge tests were conducted between cut-off potentials of 0.9 and 2.4 V (vs. Mg/Mg^{2+}) at a constant current of 60 mA g^{-1} (0.1 C rate). All electrode cells

were set up under a nitrogen atmosphere in a closed container and all measurements were conducted at room temperature (25 °C).

4.3 Results and Discussion

Figure 4-1 shows the XRD patterns of the V_2O_5 products. The pattern generated by the xerogel dried at 300 °C for 8 h (Figure 4-1c) is generally equivalent to that of crystalline V_2O_5. These results are similar to those reported by Hibino et al.[7] In contrast, the XRD patterns of the V_2O_5 xerogel irradiated with MWs for 4 min (Figure 4-1a) and the specimen dried at 200 °C for 8 h (Figure 4-1b) both exhibit a broad, intense diffraction peak around $2\theta = 7°$ and broad but weak peaks at approximately 23° and 31°, indicating structurally-preserved xerogel.[8] These peaks represent the (00l), (003) and (004) faces. The peak intensities of the MW-irradiated V_2O_5 are lower than those of the heat-treated V_2O_5, and the diffraction peaks of the former are shifted to lower angles. These results suggest that MW irradiation resulted in a lower degree of crystallinity and longer interlayer distances than conventional heat treatment, because the MWs selectively heat the water molecules in the xerogel. The interlayer distances as calculated using the Bragg equation were 11.96 and 11.58 Å following MW irradiation and heat treatment, respectively. Williamson-Hall plots of XRD peak data are provided in Figure 4-2. The slope of the plot in the case of the V_2O_5 prepared by MW irradiation is greater than that of the heat treatment sample, and so it appears that the crystal structure of the V_2O_5 prepared by MW irradiation is characterized by distorted layers. Therefore, it is believed that water of hydration is essentially instantaneously eliminated by MW irradiation.

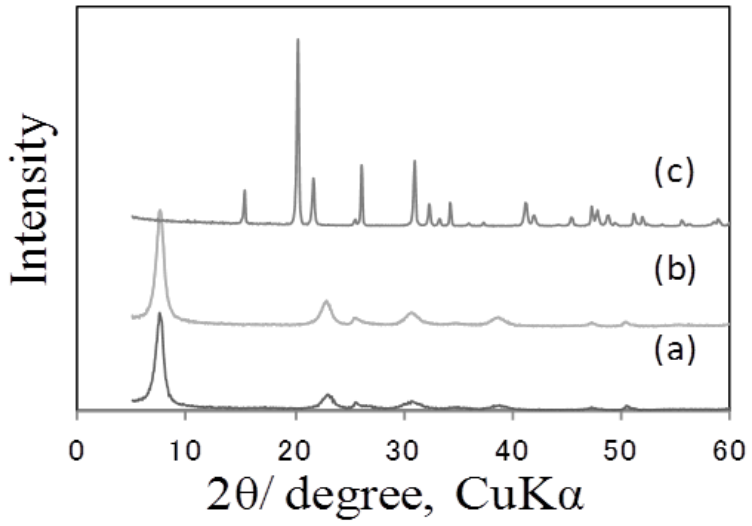

Figure 4-1 XRD patterns of vanadium pentoxides prepared by (a) MW irradiation for 4 min, (b) heat-treatment at 200 °C for 8 h, and (c) at 300 °C for 8 h.

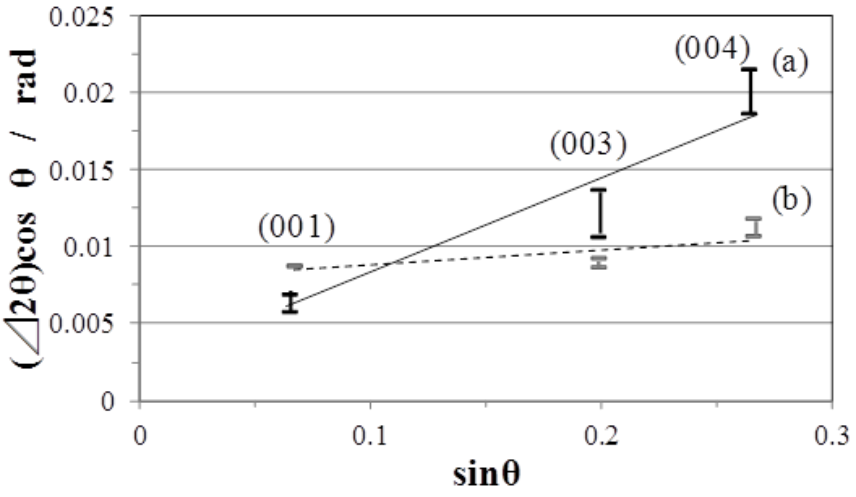

Figure 4-2 Williamson-Hall plots of V_2O_5 prepared by (a) MW irradiation and (b) heat-treatment at 200 °C. The vertical width of the plot represents a deviation.

Charge and discharge capacity curves are shown in Figure 4-3. The capacity of the crystalline V_2O_5 was 77 mAh/g (Figure 4-3(c)), a value that is similar to that reported by Yu et al.[10] The first discharge capacity of the V_2O_5 prepared by heat treatment at 200 °C was 138 mAh/g (Figure 4-3(b)) and the second discharge capacity was similar. In contrast, the first discharge capacity of the V_2O_5 prepared by MW irradiation was 175 mAh/g (Figure 4-3(a)) and the second discharge capacity was increased by a factor of 2.66 (to 463 mAh/g), presumably as the result of increased Mg^{2+} insertion following the first cycle. These results may be attributed to enhancement of the electrode surface, just as in a nickel-hydride battery, through increased interlayer distances following the first cycle insertion of Mg^{2+} ions. The theoretical capacity of the V_2O_5 xerogel was found to be 483 mAh/g and these data indicate that the interlayer distances of the V_2O_5 prepared by MW irradiation were similar to those of the V_2O_5 xerogel.

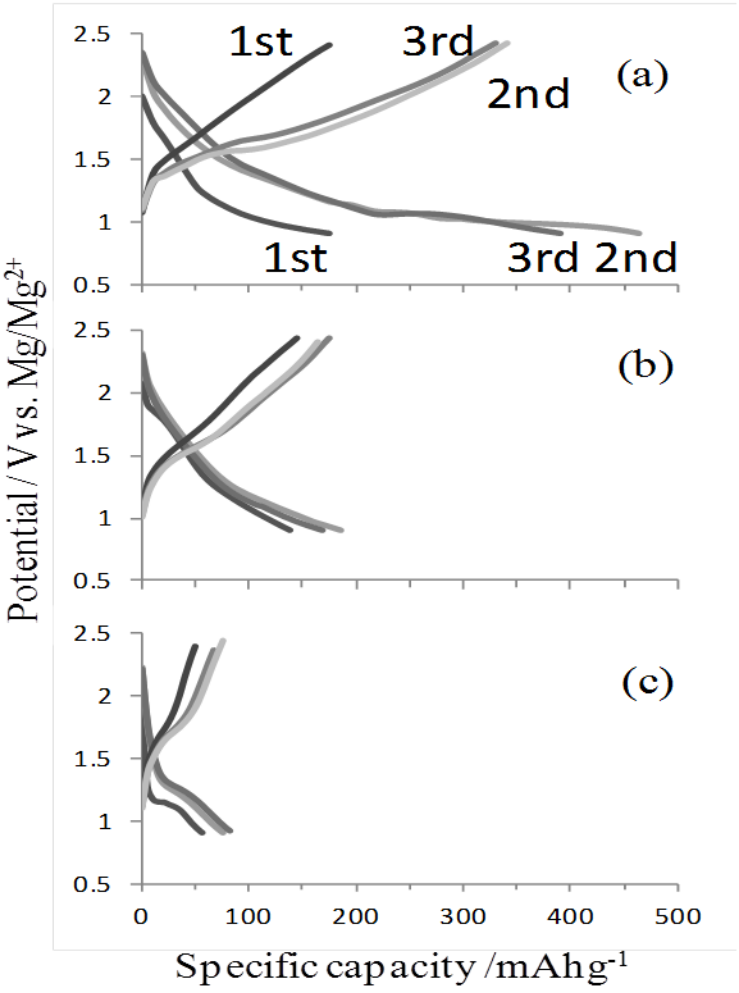

Figure 4-3 Charge-discharge curves of V_2O_5 prepared by (a) MW irradiation, (b) at 200 °C, and by (c) heat-treatment at 300 °C.

Figure 4-4 shows cyclic voltammograms obtained from the prepared xerogels. The V_2O_5 prepared by MW irradiation generated a cathodic peak at approximately -0.15 V vs. Ag/Ag+, and its cathodic response had an earlier onset compared with that of the heat-treated V_2O_5. These results demonstrate that Mg^{2+} ions were inserted into the V_2O_5 interlayers and that MW irradiation increased the number of Mg^{2+} insertion sites. In contrast, the V_2O_5 prepared by conventional heat treatment at 200 °C did not generate the same type of cathodic peak, presumably because of the short interlayer distances in this material, as previously reported by Hibino et al.[9] However, the V_2O_5 prepared at 300 °C produced a cathodic peak in the vicinity of -0.45 V, suggesting that Mg^{2+} ions were inserted near apical oxygen atoms.[6] Therefore, the CV results are consistent with the XRD and charge-discharge data.

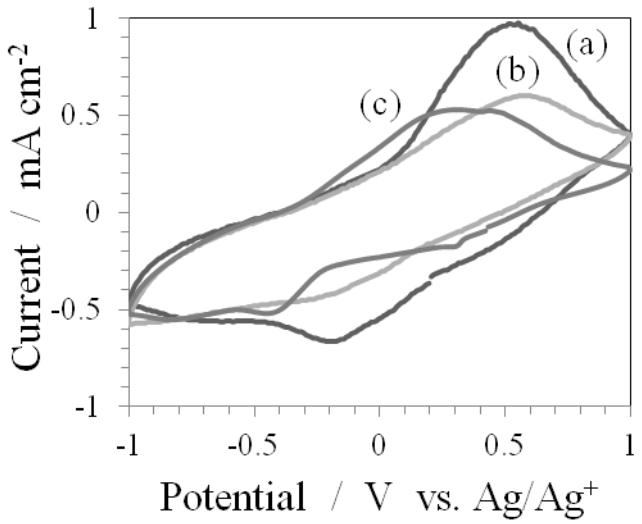

Figure 4-4 Cyclic voltammograms (1 mV s^{-1}, 2nd cycle) of V_2O_5 prepared by (a) MW irradiation, (b) heat-treatment at 200 °C and (c) heat-treatment at 300 °C.

4.4 Conclusions

A V_2O_5 xerogel prepared by MW irradiation exhibited both a low degree of crystallinity and distorted layers. Its first cycle capacity was 175 mAh/g, a value that was almost equal to that of V_2O_5 prepared by conventional heat treatment. However, the second discharge capacity of the former was 463 mAh/g, which is 2.66 times larger than that of the latter.

4.5 References of Chapter 4

1) D. Aurbach, Z. Lu, A. Schechater, Y. Gofer, R. Turgeman, Y. Cohen, M. Moshkovich and E. Levi, *Nature*, **407** (6805), 724-727 (2000)
2) D. Aurbach, Y. Cohen and M. Moshkovich, *Electrochem. Solid State Letter*, **4** (8), A113-A116 (2001)
3) P. Novak and J. Desilvestro, *J. Electrochem. Soc*, **140** (1), 140-144 (1993)
4) P. Novak, W. Scheifele and O. Haas, *J. Power Sources*, **54** (2), 479-482 (1995)
5) D. Imamura and M. Miyayama, *Solid State Ionics*, **161** (1-2),173-180 (2003)
6) M. Inamoto, H. Kurihara and T. Yajima, *Hyomen Gijutsu*, **62** (10), 516-520 (2011)
7) M. Hibino, Y. Ikeda, Y. Noguchi and T. Kudo, *Seisan Kenkyu*, **52** (11), 516-522 (2000)
8) I. Stojkovic, N. Cvjeticanin, S. Markovic, M. Mitric and S. Mentus, *Acta Physica Polonica A*, **117** (5), 837 (2010)
9) M. Hibino, Y. Ikeda and T. Kudo, *Seisan Kenkyu*, **53** (9), 432-438 (2001)
10) L. Yu and X. Zhang, *Colloid Int. Sci*. **278** (1), 160-165 (2004)
11) M. Hibino and T. Kudo, *Hyomen Gijutsu*, **36** (10), 45-53 (1998)

Chapter 5

Electrode Performance of Sulfur-Doped Vanadium Pentoxide Gel Composite Cathode Materials

5.1 Introduction

In recent years, high capacity secondary batteries have been widely adopted as power sources for electric vehicles. Magnesium secondary batteries, which have been studied for some time now, have attracted attention with regard to their use in this type of next-generation power storage application. Magnesium has several advantages since it is a low-cost material that is safe to handle, environmentally friendly, and naturally abundant. Aurbach et al. has reported an electrolyte solution that allows magnesium to be dissolved and deposited reversibly.[1,2] However, there are a limited number of materials that may be employed as the cathode in magnesium secondary batteries. Mg^{2+} may be trapped in the cathode material because of its slow solid-state diffusion. Repetitive insertion/desorption of Mg^{2+} at the cathode due to high voltages can induce structural failure of the cathode or its dissolution into the electrolyte solution. Thus, one drawback of magnesium secondary batteries is the difficulty in maintaining their cycling characteristics as their capacity fades.[3,4] For this reason, there is a high demand for cathode materials capable of facilitating stable insertion/extraction of Mg^{2+} in order to create a feasible magnesium secondary battery. The most commonly studied cathode materials are metal oxides[5,6] and metal sulfides.[7,8] As a rule, metal oxides possess stable crystal architectures but easily trap Mg^{2+}. Metal sulfides, in contrast, are less likely to trap Mg^{2+} because their structures are generally unstable. However, as sulfides generally have lower bond energies than oxides, they are thought to be unsuitable as cathode materials for lithium-ion batteries and hence may also be inadequate for magnesium batteries.

Previously, our group has reported the electrode performance of S-doped vanadium pentoxide (S-V_2O_5) prepared using a so-called carbon fiber microwave plasma (CF-MWP).[9] The capacity of this material was found to be 300 mAh/g and it was determined to consist largely of crystalline V_2O_5, but with a surface having an amorphous xerogel-like structure. This characteristic structure may be effective in enhancing electric charge transfer between the constituents of the electrode, and in allowing the facile migration of Mg^{2+}. At the time, we were concerned that the bulk crystalline V_2O_5 may not contribute to the capacity of the material. We therefore worked to transform the bulk S-V_2O_5 to a xerogel structure so as to increase its capacity. This was done by treating a V_2O_5 xerogel powder prepared by a new process with CF-MWP. This newer V_2O_5 xerogel is known to exhibit particularly high capacity due to the spread-out structure of the layers and the associated inclusion of structural water in the interlayers. The resulting xerogel has a maximum theoretical capacity of 1030 mAh/g based on the formula $V_2O_5 \cdot 6H_2O$, which includes the maximum amount of structural water. We have previously reported that this V_2O_5 xerogel, following irradiation with microwaves under reduced pressure, exhibits a capacity of 600 mAh/g, although this capacity is decreased significantly with repeated cycling.[10] A V_2O_5 xerogel prepared by the conventional sol-gel method results in plate-like particles, making it difficult to obtain a mixture of the xerogel and sulfur powder, but this problem is avoided with our new technique. The structure and electrode characteristics of material generated by our new process were examined in this work, and the results are presented herein.

5.2 Experimental

5.2.1 Preparation method for key cathode material: sulfur-containing V_2O_5 gel

Acetone (10 mL) was added to a 10 wt% aqueous H_2O_2 solution (100 mL), after which V_2O_5 (1 g) was dispersed in the mixture with electromagnetic stirring. As noted, the plate-like V_2O_5 xerogel particles normally generated by the sol-gel method make it difficult to mix in sulfur powder. However, the addition of acetone to the sol-gel mixture resulted in the rapid synthesis of particles of V_2O_5 xerogel. Upon addition of the V_2O_5, bubbling of the solution was observed, followed soon after by explosive boiling and the immediate precipitation of the V_2O_5 gel. This gel was filtered, collected and dried at 80 °C, and subsequently mixed with sulfur powder (molar ratio 2:1) for 20 min in a ball mill at 500 rpm (P-6, Fritsch Co., Ltd.). The resulting composite was wetted and left to sit overnight, after which treatment with CF-MWP was carried out. Specifically, a sample of the raw material (0.5 g) was placed between two pieces of carbon felt (30 mm in diameter) and a 500 W 2.45 GHz microwave source was used to irradiate the material under reduced pressure (0.001 MPa) for 2 min (Figure 5-1) to synthesize the hybrid cathode material. This process involves treatment of the raw material with a plasma formed from the water contained in the material itself as a result of electric discharges between the pieces of carbon felt. It was assumed that the water in the sample being treated was distributed in a sufficiently uniform manner so as to ensure that treatment of the composite was uniform. Although this process was performed under reduced pressure and at the evaporation temperature of water, it was later confirmed that the treatment did not induce reduction of the V_2O_5 or oxidation of the sulfur. For

comparison purposes, a composite of V_2O_5 gel and sulfur was calcined at 250 °C. The structure of the S-V_2O_5 gel was examined by X-ray diffraction (XRD; Rigaku, SmartLab), scanning electron microscopy (SEM; Hitachi, SU3500) and thermogravimetry-differential thermal analysis (TG-DTA; Rigaku, TG8120).

5.2.2 Electrochemical analysis

Electrodes were prepared using a 7:2:1 (by mass) mixture of the cathode material, acetylene black and polyvinylidene fluoride (PVDF) binder in N-methyl-2-pyrrolidone as the solvent. The resulting slurry was spread on carbon paper to a density of 2 mg cm^{-2} to form an electrode that was then dried at 110 °C for 1.5 h.

Cyclic voltammetry (CV) analysis with three electrode cells to assess the electrode performance was conducted using an electrochemical measurement system (Hokuto Denko, HZ-3000) with Ag/AgCl as the reference electrode and a platinum counter electrode. A propylene carbonate (PC) solution containing 0.3 M $Mg(ClO_4)_2$ and 1.8 M H_2O was used as the electrolyte, since this solution has been shown to allow smooth charges and discharges when employed with metal oxides.[3] The sweep rate was 0.5 mV s^{-1} and the sweep range was between -2.0 and +0.5 V. Charge-discharge tests were conducted at cut-off potentials from 2.6 to 0.9 V versus Mg/Mg^{2+} at a constant current of 21 $mA^{/}g$ (C/15 rate). In some trials, a theoretical capacity limit of 450 mAh/g was applied in addition to the cut-off potential. In these cases, magnesium ribbon (Nilaco) was used as the reference electrode. An S-V_2O_5 electrode prepared using CF-MWP and charged with magnesium ions was used as the counter electrode.[9,11] This electrode exhibited the same potential changes as a magnesium alloy plate. All measurements were conducted at 30 °C.

5.3 Results and discussion

5.3.1 Structural analysis

Employing the traditional sol-gel method to produce the V_2O_5 xerogel typically gives a reddish-brown sol following vigorous boiling of the synthesis solution. However, the addition of acetone in the present modified method resulted in the precipitation of a dark green V_2O_5 gel. A portion of the V in this gel may therefore have undergone reduction from the +5 to the +4 state.

Figure 5-1 shows the XRD patterns of (a) the V_2O_5 gel, (b) the S-V_2O_5 composite produced by mixing the V_2O_5 gel with sulfur, (c) the S-V_2O_5 composite after heat treatment at 250 °C and (d) the S-V_2O_5 gel obtained from CF-MWP treatment. The XRD pattern of the V_2O_5 gel (Figure 5-1(a)) contains a 001 peak and hk0 indexed peaks, indicating that the planar structure was stacked in the vertical direction. The XRD pattern of the sulfur mixture (Figure 5-1(b)) has a 001 peak that is broader than that generated by the V_2O_5 gel, and also exhibits peaks attributed to S_8. In the XRD pattern of the S-V_2O_5 composite after heat treatment at 250 °C (Figure 5-1(c)), this S_8 pattern has disappeared. The XRD pattern of the S-V_2O_5 gel (Figure 5-1(d)) exhibits the same broad peaks as the V_2O_5 gel in addition to low intensity S_8 peaks, suggesting that the S-V_2O_5 gel is almost amorphous.

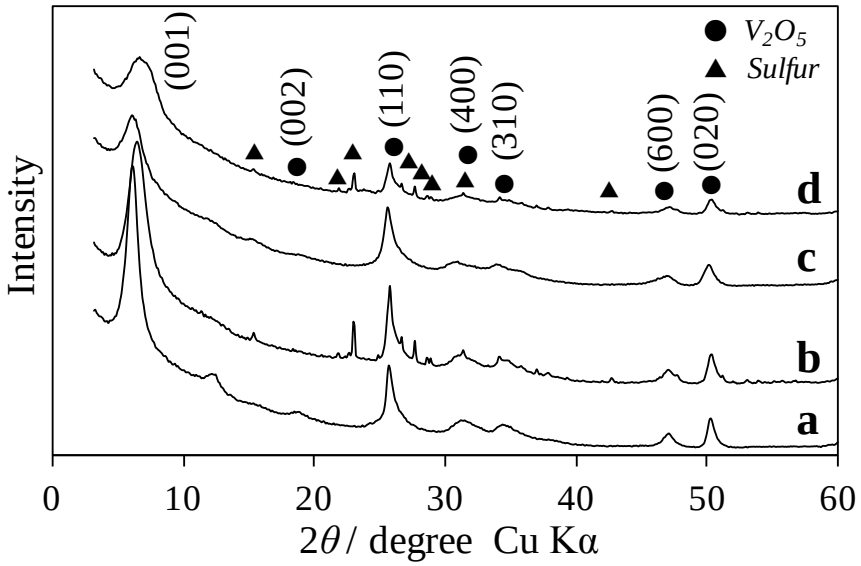

Figure 5-1 XRD patterns of (a) V_2O_5 gel, (b) V_2O_5-sulfur composite, (c) V_2O_5-sulfur composite after heat-treatment at 250 °C for 8 h, and (d) S-V_2O_5 gel.

Figure 5-2 presents the TG-DTA data obtained from (a) the S-V_2O_5 composite, (b) the S-V_2O_5 composite after heat treatment at 250 °C and (c) the S-V_2O_5 gel. The left hand y axis indicates mass loss (that is, the TG data) while the right hand y axis shows heat flow (the DTA data). The TG-DTA results for the S-V_2O_5 composite (Figure 5-2(a)) demonstrate mass loss both below 100 °C and from 175 to 225 °C, in addition to an exothermic peak ranging from 175 to 225 °C. The decrease in mass below 100 °C was most likely the result of the desorption of structural water from the V_2O_5 gel. The elimination of sulfur began at 175 °C and continued until 225 °C, as indicated by the 26% mass loss, a value that equaled the proportion of sulfur in the mixture. Analysis of the S-V_2O_5 composite after heat treatment at 250 °C (Figure 5-2(b)) showed no peaks. In contrast, the data obtained from the S-V_2O_5 gel (Figure 5-2(c)) exhibits an exothermic reaction from 170 to 185 °C, indicating sulfur elimination beginning at 170 °C and ending at 185 °C. The TG results for the S-V_2O_5 gel also show a significant decrease in mass above 300 °C. Explosive collapse occurred above 300 °C, such that the V_2O_5 gel particles were observed to burst within the measurement chamber. Such thermal behavior is often observed in materials that have a hard amorphous structure at the periphery.

Figure 5-3 presents SEM images of (a) the S-V_2O_5 mixture, (b) the S-V_2O_5 composite after heat treatment at 250 °C and (c) the S-V_2O_5 gel. The V_2O_5 gel evidently formed rod-like crystals. Although the V_2O_5 was expected to undergo crystal growth in a planar format, crystal growth was inhibited in the V_2O_5 gel due to the synthesis method applied. The S-V_2O_5 composite after heat treatment at 250 °C (Figure 5-3(b)) has a layered structure. From these results, it is evident that the V_2O_5 gel had an amorphous structure, because the elimination of sulfur was accompanied by instability in the gel. The S-V_2O_5

gel (Figure 5-3(c)) was found to contain angular particles. These data show that the periphery of the S-V_2O_5 gel was made amorphous during treatment with the CF-MWP, leading to explosive collapse of the gel, as observed by TG-DTA, with the formation of an angular morphology at the surface.

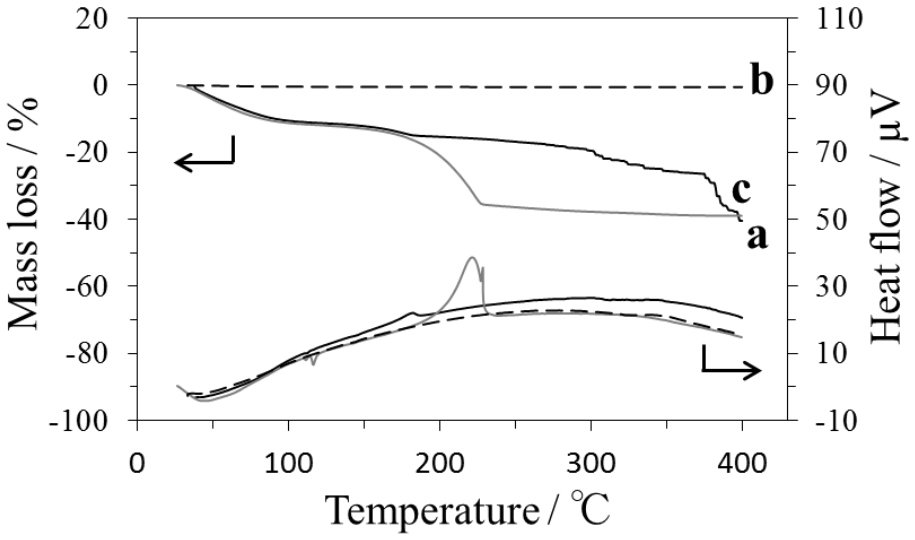

Figure 5-2 TG-DTA of (a) V_2O_5-sulfur composite, (b) V_2O_5-sulfur composite after heat treatment at 250 °C for 8 h, and (c) S-V_2O_5 gel.

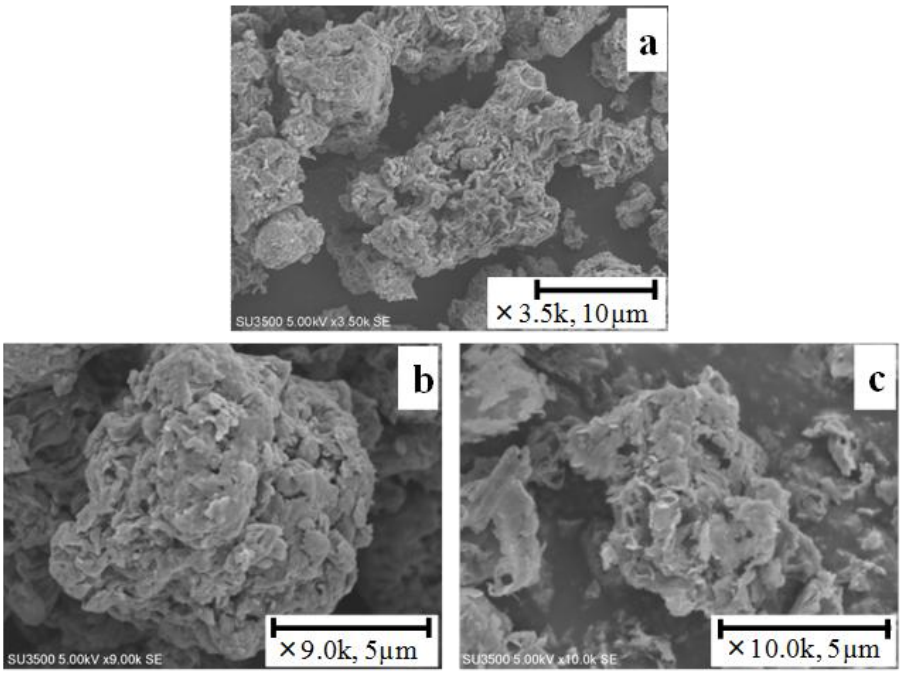

Figure 5-3 SEM images: (a) V_2O_5-sulfur composite, (b) V_2O_5-sulfur composite after heat treatment at 250 °C for 8 h, and (c) S-V_2O_5 gel.

5.3.2 Electrochemical analysis

Figure 5-4(a) presents cyclic voltammograms (CV) obtained from the V_2O_5 gel. There are three anodic peaks at 0, -0.7 and -1.3 V, and three cathodic peaks at -0.9, -0.35 and 0.2 V. The intensity of each of the peaks decreased as the cycles progressed. Figure 5-4(b) shows CVs generated by the S-V_2O_5 gel. During the first cycle, two anodic peaks were produced at -0.8 and -1.25 V, and two cathodic peaks at -0.6 and -0.05 V. During the second cycle, two anodic peaks were generated at -0.8 and -1.25 V, and two cathodic peaks at -0.6 and -0.3 V, and the CV characteristics stabilized after the second cycle. The anodic peaks at 0 and -0.7 V and the cathodic peaks at -0.9 and -0.35 V obtained from the V_2O_5 gel and all peaks produced by the S-V_2O_5 gel can likely be attributed to the V_2O_5 xerogel. The anodic and cathodic peaks observed at 0 and 0.2 V in the case of the V_2O_5 gel are very weak in the S-V_2O_5 gel pattern, likely as a result of changes in the layer state induced by the CF-MWP treatment. The XRD pattern of the S-V_2O_5 gel shows the disappearance of the peak attributed to the (002) faces, possibly due to insertion/extraction at sites that are attributed to (002) faces. As discussed earlier, the S-V_2O_5 gel has an amorphous layer at its periphery due to the CF-MWP treatment. It is interesting to note that the S-V_2O_5 gel was activated by the first cycle, similar to the behavior of the electrode in a nickel hydride battery, with resulting stabilization after the second cycle.[12)] This similarity to a nickel hydride battery suggests that the interlayer distance is increased by the first cycle insertion of Mg^{2+} ions.

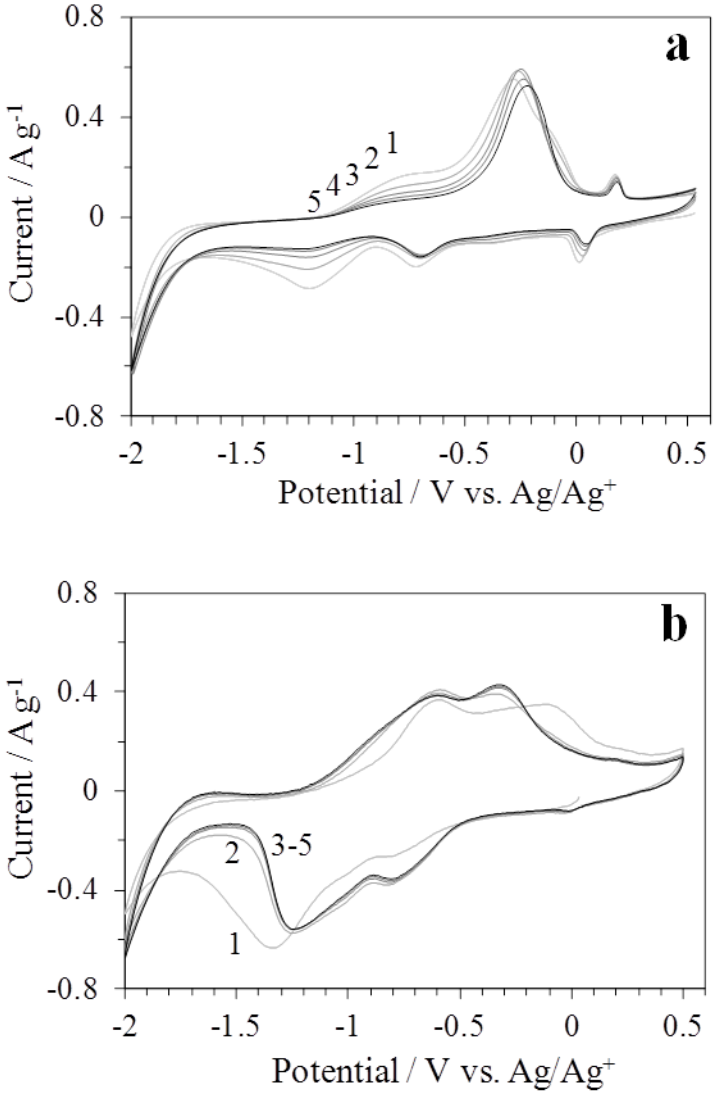

Figure 5-4 Cyclic voltammograms of (a) V_2O_5 gel and (b) S-V_2O_5 gel.

Charge and discharge capacity curves are shown in Figure 5-5. A plateau was generated at 1.4 V and the capacity of the S-V_2O_5 gel was found to be 450 mAh/g after several cycles, likely due to the V_2O_5 gel because the potential of sulfur is approximately 1.0 V versus Mg/Mg^{2+}. The linear decrease in the potential suggests that the S-V_2O_5 gel had an amorphous structure, as has also been reported by Funabiki et al.[13,14] A small potential plateau appears at 1.95 V after the second cycle and this is in agreement with the CV results for the S-V_2O_5 gel, which is believed to have a hard amorphous surface structure due to the added sulfur and the CF-MWP treatment. This structure possibly inhibits the insertion of ligands with Mg^{2+} at the interlayer, which suggests a solution to the challenges associated with the V_2O_5 xerogel. Although the charge overpotential was increased, the cycling characteristics of this material require further improvement.

The V_2O_5 gel obtained in this work had a planar structure that was layered in the vertical direction and its inner layers contained structural water, similar to a V_2O_5 xerogel. When this gel was treated with CF-MWP after mixing with sulfur, planar layers stacked in the vertical direction extended across much of the gel, forming a xerogel-like amorphous structure at the inner core of the S-V_2O_5 gel, distinct from crystalline V_2O_5. This may be the reason for the high capacity of the S-V_2O_5 gel.

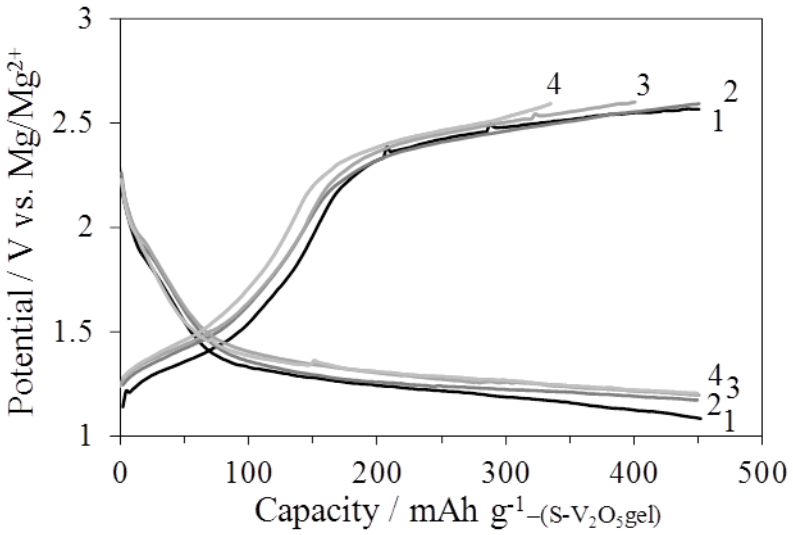

Figure 5-5 Charge-discharge curves for S-V_2O_5 gel.

5.4 Conclusions

This work successfully synthesized a V_2O_5 gel using a novel method in which acetone and V_2O_5 were added to an aqueous H_2O_2 solution. The XRD pattern of the V_2O_5 gel showed a 001 peak and hk0 indexed peaks, indicating a planar structure stacked in the vertical direction. A S-V_2O_5 gel was subsequently obtained by treating a composite of the V_2O_5 gel and sulfur with CF-MWP. The bulk of the S-V_2O_5 gel consisted of V_2O_5 gel and sulfur, and the surface had an amorphous structure. The capacity of the S-V_2O_5 gel was 450 mAh/g.

The effects of the addition of sulfur can be summarized as follows: (1) the transfer of electric charge between sulfur and the V_2O_5 became smoother and faster and (2) the transfer of Mg^{2+} was facilitated owing to the transformation of the periphery of the S-V_2O_5 gel to an amorphous form after CF-MWP treatment. An extensive study of the mechanism of the electrochemical behavior of the S-V_2O_5 electrode is now in progress. Furthermore, the S-V_2O_5 gel is expected to show higher performance (that is, higher capacity, higher potential and improved cycling characteristics) when doped with magnesium or a transition metal such as nickel.

5.5 References of Chapter 5

1) D. Aurbach, Z. Lu, A. Schechter, Y. Gofer, H. Gizbar, R. Turgeman, Y. Cohen, M. Moshkovich and E. Levi, *Nature*, **407** (6805), 724-727 (2000)
2) D. Aurbach, Y. Cohen and M. Moshkovich, *Electrochem. Solid-State Lett.*, **4** (8), A113-A116 (2001)
3) P. Novák, W. Scheifele, F. Joho and O. Haas, *J. Electrochem. Soc.*, **142** (8), 2544-2550 (1995)
4) P. Novák, W. Scheifele and O. Haas, *J. Power Sources*, **54** (2), 479-482 (1995)
5) P. Novák and J. Desilvestro, *J. Electrochem. Soc.*, **140** (1), 140-144 (1993)
6) Z. Feng, J. Yang, Y. NuLi and J. Wang, *J. Power Sources*, **184** (2), 604-609 (2008)
7) Z. L. Tao, L. N. Xu, X. L. Gou, J. Chen and H. T. Yuan, *Chem. Commun. (Camb)*, (18), 2080-2081 (2004)
8) A. Mitelman, M. D. Levi, E. Lancry, E. Levi and D. Aurbach, *Chemical Communications*, (41), 4212-4214 (2007)
9) M. Inamoto, H. Kurihara and T. Yajima, *Hyomen Gijutsu*, **62** (10), 516-520 (2011)
10) M. Inamoto, H. Kurihara and T. Yajima, *Electrochemistry*, **80** (6), 421-422 (2012)
11) M. Inamoto, H. Kurihara and T. Yajima, *Materials*, **6** (10), 4514-4522 (2013)
12) F. C. Ruiz, H. A. Peretti, A. Visintin and W. E. Triaca, *Int. J. Hydrogen Energy*, **36** (1), 901-906 (2011)
13) A. Funabiki, H. Yasuda and M. Yamachi, *Electrochemistry*, **12** (71), 1081-1083 (2003)
14) H. Morimoto, D. Ikeda, A. Hayashi, M. Tatsumisago and T. Minami, *Electrochemistry*, **12** (71), 1036-1038 (2003)

Chapter 6

General Conclusions

This work examined the feasibility of using a V_2O_5/sulfur composite as a magnesium secondary battery cathode, with the aim of developing a cathode material that would allow the repeated insertion/extraction of Mg^{2+} ions and would exhibit high capacity.

As reported in Chapter 2, a V_2O_5/sulfur synthesized by CF-MWP (S-V_2O_5) showed a capacity of 300 mAh/g. It was found that the S-V_2O_5 particles were composed of two parts; an inner core of rigid V_2O_5 crystals covered by an approximately 10 nm thick surface layer similar to a V_2O_5 xerogel and incorporating sulfur. XPS analysis of the S-V_2O_5 electrode surface after charge and discharge indicated the presence of an electrolyte layer, representing a so-called solid electrolyte interphase (SEI), formed at the interface between the electrolyte and the S-V_2O_5 electrode surface. This SEI plays an important role in promoting the solid-state diffusion of Mg^{2+} ions.

Chapter 3 reported the ability of S-V_2O_5 to achieve high capacity when combined with a metal oxide. The highest recorded capacity (420 mAh/g) was obtained upon the addition of MnO_2 to form the composite SMn-V_2O_5. Structural assessments showed that

the bulk of the SMn-V_2O_5 had an orthorhombic V_2O_5 structure, while the surface was composed of xerogel-like V_2O_5 and a solid solution of MnO_2 and sulfur.

Chapter 4 summarized work to prepare a V_2O_5 xerogel by microwave irradiation and the results of structural and electrochemical properties assessments. X-ray diffraction showed that the V_2O_5 xerogel prepared by microwave irradiation had a low degree of crystallinity, while charge-discharge tests revealed a specific capacity of 463 mAh/g.

In Chapter 5, the preparation of a S-V_2O_5 gel using a new process and subsequent evaluation of the structure and electrode performance is discussed. Structural analysis showed that the bulk S-V_2O_5 gel adopted a V_2O_5 xerogel-like structure with a surface layer incorporating the sulfur and in a stable planar orientation, and that the surface had a reformed hard amorphous structure due to the CF-MWP treatment. Charge-discharge tests determined a specific capacity of 450 mAh/g, and cyclic voltammetry found almost perfect stability after the second cycle.

From these results, the S-V_2O_5 composite can be expected to function as a cathode material via Mg^{2+} ion insertion/extraction based on its enhanced cycling ability and structural stability. This study did not undertake a detailed analysis of the sulfur states in the S-V_2O_5, although such states are believed to have a significant effect on ion insertion/extraction. In future work, the effect of sulfur states on Mg^{2+} ion insertion/extraction should be assessed. The results herein demonstrate the feasibility of using magnesium secondary batteries for practical applications based on further advances in the anode and electrolyte.

Future work should focus on enhancing the cycling characteristics of the cathode, by inhibiting dissolution of the sulfur in the S-V_2O_5, and should analyze the sulfur states in

S-V_2O_5. Together with additional work regarding the electrolyte and anode, such studies should allow the practical realization of magnesium secondary batteries.